types of abnormal rhodopsin proteins can be misfolded and retained in ER; in some cases, the mutant proteins are bound by the ER-resident chaperone, BiP [3]. The accumulated mutant proteins may induce unfolded-protein response (UPR) to alleviate the ER stress. In general, the abnormal proteins could be degraded through ubiquitin proteasome pathway and/or autophagy [4]. However, if the mutant protein was overloaded, the prolonged UPR will induce ER stress-associated programmed cell death, apoptosis [5]. Although many *rhodopsin* gene abnormalities are believed to be related to ER stress [3], practical therapies targeting mutant rhodopsin proteins or downstream signaling pathways have yet to be established. This may be due, in part, to the insufficient understanding of the disease pathogenesis: mutations associated with RP are genetically heterogeneous, and, in most cases, there is no formal proof of a causal relationship between the genetic mutation and the RP phenotype. Furthermore, only a limited number of genetic abnormalities have been reproduced and studied in *Drosophila* [6] and mouse systems [7,8], and drug screening is not easily performed due to the lack of appropriate screening systems. Although the abnormal gene of interest can be expressed in cell lines, overexpression commonly results in artificial cellular responses.

In an effort to develop an authentic cell-based model of human RP, induced pluripotent stem cell (iPSC) technology [9,10] has been recently applied to this disorder [11,12]. However, a causal relationship between genetic mutations and the RP phenotype remains to be elucidated. In the present study, we generated iPSCs from the somatic cells of an RP patient carrying a heterozygous mutation in the *rhodopsin* gene [13]. These cells were then differentiated into rod photoreceptor cells to investigate the cellular pathogenesis of RP and to screen chemical therapeutics. A comparison of the RP and control iPSC-derived photoreceptor cells showed that the RP patient's iPSC-derived rod photoreceptor cells had a reduced survival rate in culture and an increased ER stress response. Furthermore, to formally demonstrate that the phenotype was due to the expression of mutant rhodopsin, we utilized the helper-dependent adenoviral vector (HDAdV) to replace the mutated *rhodopsin* gene in the RP patient's iPSCs with the wild-type *rhodopsin* gene, thus repairing the gene, and found that the phenotype of the iPSC-derived photoreceptor cells reverted to normal. This method allowed a phenotypic comparison between the iPSC-derived photoreceptor cells of the same genetic background and developmental course during iPSC generation. Moreover, replacing the wild-type gene in the control iPSCs with a mutated gene using HDAdV reconstructed the pathological condition. We next used the RP patient's iPSC-derived photoreceptor cells to screen for chemical reagents that rescued the ER stress phenotype. The involvement of autophagy, which can be induced in response to ER stress [14], was also explored.

Results

Generation of iPSCs from an RP patient

The iPSC line RP#5 (#5) was generated using skin cells [15] isolated from an RP patient carrying a *rhodopsin* mutation (a G to A substitution at nucleotide 541) (Figure 1A) [13]. The point mutation resulted in a change in amino acid 181 from a glutamic acid (E) to lysine (K) (E181K) and was shown to be present on one allele in the #5 iPSCs but not in the 201B7 (B7) iPSCs (Figure 1B). The expression of pluripotent markers (Figure 1C-E) and the formation of teratomas containing all three germ layer cells (Figure 1F) were also confirmed.

Preparation of gene-targeted iPSC lines

To determine whether the expression of rhodopsin E181K was solely responsible for the accelerated photoreceptor cell loss, we prepared *rhodopsin* gene-targeted iPSCs using HDAdVs. A wild-type *rhodopsin* gene in a BAC clone, with a *Neo* cassette introduced in the third intron, was inserted into an HDAdV vector to generate the correction vector (Figure 2A). Using this correction vector, the wild-type *rhodopsin* gene was replaced with the genome sequence of the #5 iPSCs through homologous recombination, followed by the removal of the *Neo* cassette by Cre recombinase to generate #5Rw iPSCs (Figure 2A). Similarly, the mutated *rhodopsin* sequence obtained from the genome of the #5 iPSCs was inserted into an HDAdV vector to construct a mutagenesis vector (Figure 2B) that was transferred into the genome of B7 iPSCs, followed by the removal of the *Neo* cassette, to generate B7Rm iPSCs (Figure 2B).

The introduction and removal of the *Neo* cassette at the *rhodopsin* locus were confirmed by PCR analyses (Figure 2C). We further confirmed the absence of the *rhodopsin* point mutation in the #5Rw cells and the presence of the heterozygous point mutation in the B7Rm cells (Figure 2D). These data indicated that the targeted *rhodopsin* gene correction and mutagenesis were successful.

Impact of the *rhodopsin* gene mutation in differentiated rod photoreceptor cells derived from iPSC lines

Next, we induced retinal cell differentiation using the serum-free embryoid body (SFEB) method, along with subsequent stepwise changes in the culture medium for several weeks, as previously reported and modified by Lamba et al. [16]. iPSCs were cultured in the presence of Noggin, Dkk-1, and IGF-1 for 3 weeks, followed by 2 weeks of culture in their absence [16]. Using this method, up to 10% of the differentiated cells were reported to express early markers of photoreceptor differentiation at the end of 3 weeks, and these cells can be transplanted into subretinal

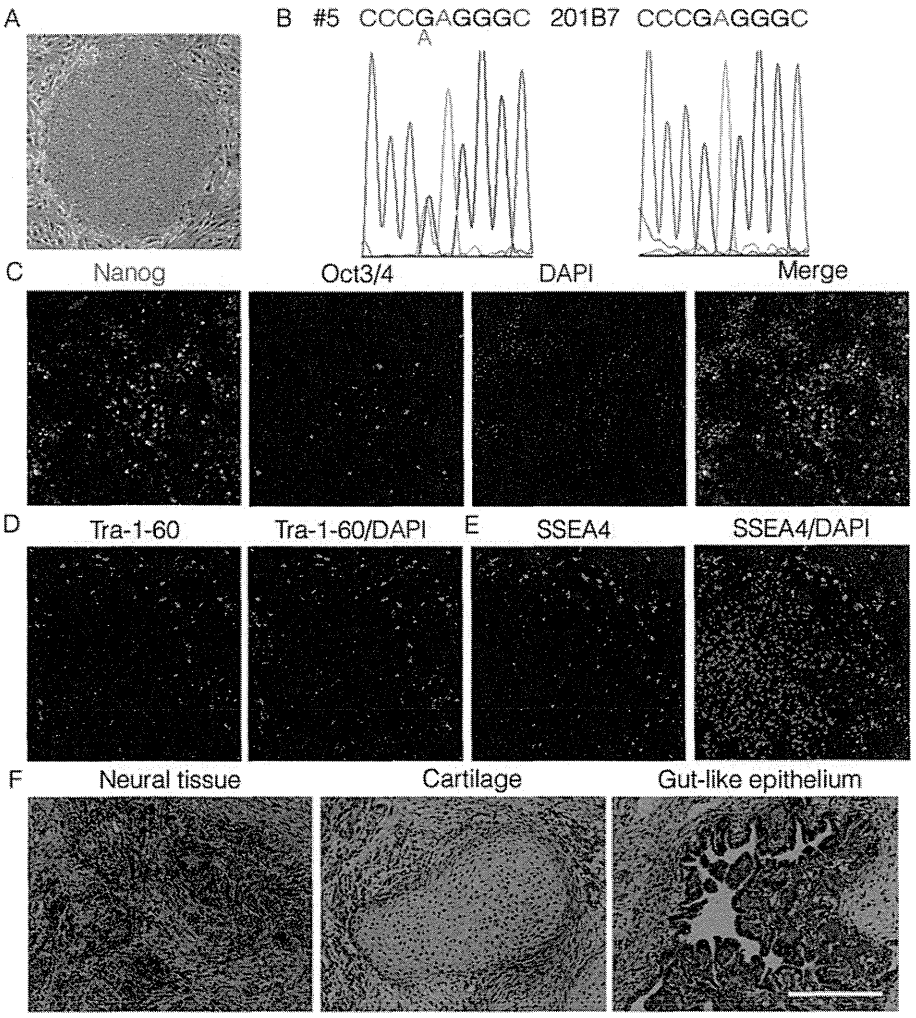

Figure 1 RP patient's iPSCs. (A) A colony of RP#5 iPSCs derived from an RP patient's skin cells. **(B)** DNA analysis of the *rhodopsin* gene in the RP#5 iPSCs and control 201B7 iPSCs. **(C-E)** Immunostaining for pluripotent markers; the nuclei were counterstained with DAPI (blue). **(C)** Nanog and Oct3/4. **(D)** Tra-1-60. **(E)** SSEA4. **(F)** Teratoma formation assay showing that the RP#5 iPSCs gave rise to all three germ layers, confirming their pluripotency. Scale bar, 1 mm **(A)**, 250 μm **(C-F)**.

space where they will integrate into the retina to form synapses [16-18]. In the present study, a recombinant adenovirus expressing EGFP under the control of the *neural retina leucine zipper* promoter, a rod photoreceptor-specific marker that acts as a transcription factor for the *rhodopsin* gene, (Ad-p*Nrl*-EGFP) [19-21], was introduced 2 days before flow cytometry analyses (Figure 3A, B). The specific detection of EGFP by flow cytometry was confirmed using the cells with (Figure 3C right) and without Ad-p*Nrl*-EGFP infection (Figure 3C left). This experiment also confirmed that 32.8% of the cells were Ad-p*Nrl*-EGFP positive after 5 weeks of culture. Among the Ad-p*Nrl*-EGFP-positive cells derived from the #5 iPSCs, we confirmed that recoverin, a photoreceptor marker, was up-regulated after 5 weeks in differentiation culture compared to the non-differentiated #5 iPSCs (Figure 3D).

Using this method, rod photoreceptor cells derived from each iPSC line (#5, #5Rw, B7, and B7Rm) were quantified weekly from 2 to 5 weeks after differentiation was initiated (Figure 3E). During the first 4 weeks of culture, the proportion of Ad-p*Nrl*-EGFP-positive rod photoreceptor cells gradually increased with time, and there was no difference among the cell lines. However, after 5 weeks in differentiation culture, the proportion of rod photoreceptor cells was significantly higher in the cultures derived from the #5Rw and B7 iPSC lines, which did not contain the mutated *rhodopsin* coding sequences, compared to the #5 and B7Rm lines, which did contain the mutation (Figure 3E, F). Furthermore, we investigated the ratio of apoptotic cells of p*Nrl*-EGFP-positive rod photoreceptor cells derived from #5 and #5Rw iPSCs, by immunostaining using an anti-Annexin V antibody (Figure 3G) and by PI

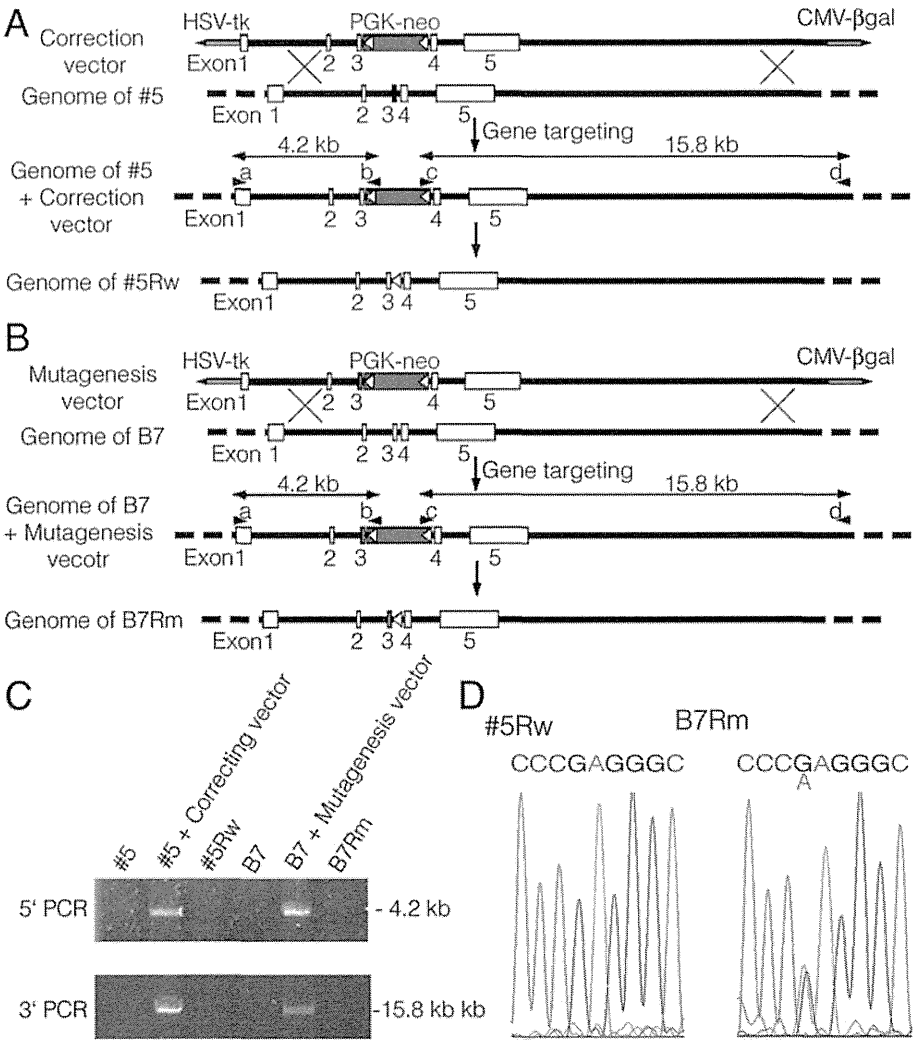

Figure 2 The *rhodopsin* gene-targeting methods. (A, B) Schematic illustrations of the *rhodopsin* gene correction implemented in the RP#5 iPSCs and the mutagenesis in the 201B7 iPSCs using HDAdVs. **(C)** A PCR analysis confirmed that recombination occurred at the *rhodopsin* locus. Products of 4.2 kb and 15.8 kb were obtained using primers a-b and c-d (arrowheads in **A**, **B**), respectively. **(D)** Sequence analysis of the recombinant *rhodopsin* genes in each iPSC line. HDAdV, helper-dependent adenoviral vector; HSV-tk, herpes simplex virus thymidine kinase gene cassette; *Neo*, neomycin-resistance gene cassette; white triangles, loxP sites; red boxes, exon 3 of *rhodopsin* containing the E181K mutation. #5, RP#5 iPSCs; #5Rw, *rhodopsin* gene-corrected RP#5 iPSCs; B7, 201B7 iPSCs; B7Rm, *rhodopsin* gene-mutated 201B7 iPSCs.

staining (Figure 3H). The p*Nrl*-EGFP-positive cells derived from #5 iPSCs included more apoptotic cells than those derived from #5Rw iPSCs, suggesting that the lower number of the rod differentiated photoreceptor cells derived from #5 than from #5Rw iPSCs was caused, at least in part, by the enhanced apoptosis of rod photoreceptor cells derived from #5 iPSCs. These data collectively indicated that the *rhodopsin* E181K mutation was solely responsible for the rod photoreceptor cell loss associated with this patient.

Because ER stress has been implicated in the pathogenesis of RP that involves *rhodopsin* mutations [3], we analyzed the expression of the ER stress markers BiP (Figure 3I) and CHOP (Figure 3J) using real-time PCR analyses. For this purpose, we purified the Ad-p*Nrl*-EGFP cells using flow cytometry and extracted mRNA from the Ad-p*Nrl*-EGFP-positive rod photoreceptor cells. The mRNA levels of both BiP and CHOP were elevated in the #5 and B7Rm iPSC-derived rod photoreceptor cells after 5 weeks in differentiation culture. Furthermore, we also examined the apoptosis-related molecules BID (Figure 3K) and NOXA (Figure 3L). After 5 weeks of culture, these molecules were also upregulated in the purified Ad-p*Nrl*-EGFP-positive rod photoreceptor cells derived from the #5 and B7Rm iPSCs, suggesting that the mutant rhodopsin protein induced ER stress and apoptosis.

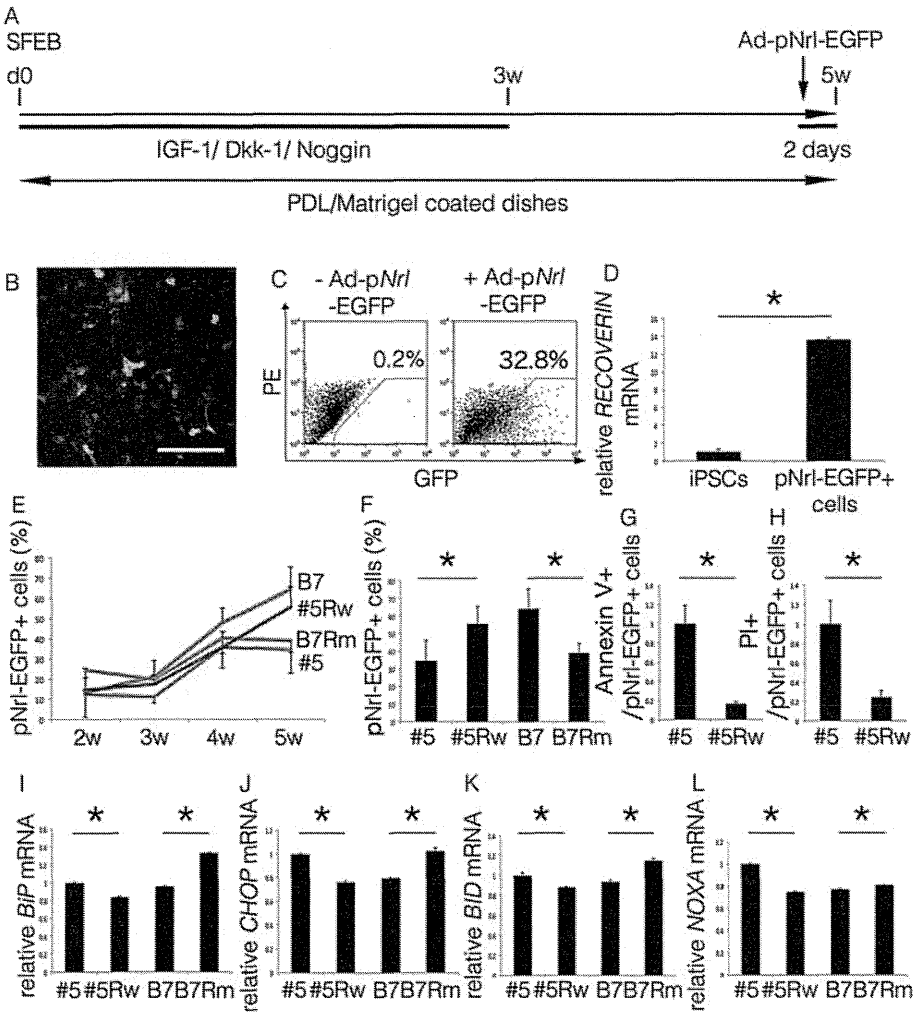

Figure 3 Impact of the E181K *rhodopsin* gene mutation on rod photoreceptor cells derived from iPSC lines. (A) Protocol of rod photoreceptor cell differentiation. **(B)** Expression of the rod photoreceptor cell-specific gene *Nrl* was visualized by infection with the Ad-p*Nrl*-EGFP virus. **(C)** Flow cytometry analysis of the differentiated cells without (left) and with (right) Ad-p*Nrl*-EGFP infection at 5 weeks. **(D)** The *recoverin* mRNA levels of the flow cytometry-purified p*Nrl*-EGFP-positive rod photoreceptor cells derived from the #5 iPSCs compared to the undifferentiated #5 iPSCs at the same time point. **(E)** Quantification of the p*Nrl*-EGFP-positive rod photoreceptor cells in each iPSC line after 2, 3, 4, and 5 weeks of differentiation. Red, B7; blue, #5Rw; pink, B7Rm; green, #5. N = 9. **(F)** Proportion of p*Nrl*-EGFP-positive rod photoreceptor cells derived from iPSC lines after 5 weeks. N = 9. **(G, H)** The ratio of dead cells in p*Nrl*-EGFP-positive photoreceptor cells detected by Annexin V **(G)** and PI **(H)**. N = 4. (I-L) Relative mRNA levels of BiP **(I)**, CHOP **(J)**, BID **(K)**, and NOXA **(L)** normalized to b-Actin in the p*Nrl*-EGFP-positive cells collected after 5 weeks, as determined by a real-time PCR analysis. N = 3. Ad-p*Nrl*-EGFP, adenovirus promoter *Nrl*-EGFP. *p < 0.05. Scale bar, 40 μm. Mean ± SD (with each p-values of marked by *) for iPSCs and p*Nrl*-EGFP cells in **(D)** 1 ± 0.38, 13.6 ± 0.14 (p = 0.049); for #5, #5Rw, B7, B7#Rm in **(F)** 34.6 ± 11.7, 55.7 ± 10.0 (p = 0.035), 64.3 ± 11.3, 38.9 ± 5.8 (p = 0.013); for #5 and #5Rw in **(G)** 1 ± 0.18, 0.16 ± 0.02, (p = 0.019) **(H)** 1 ± 0.24, 0.24 ± 0.07 (p = 0.021); for #5, #5Rw, B7, B7#Rm in **(I)** 1 ± 0.005, 0.83 ± 0.002 (p < 0.0001), 0.95 ± 0.006, 1.33 ± 0.004 (p < 0.0001); **(J)** 1 ± 0.002, 0.76 ± 0.007 (p < 0.0001), 0.79 ± 0.005, 1.03 ± 0.010 (p < 0.0001); **(K)** 1 ± 0.016, 0.88 ± 0.006 (p = 0.003), 0.94 ± 0.008, 1.14 ± 0.013 (p < 0.0001); **(L)** 1. ± 0.005, 0.75 ± 0.005 (p < 0.0001), 0.77 ± 0.005, 0.80 ± 0.004 (p = 0.001). All statistical analyses in this figure were carried out by Student's T test.

Drug screening using rod photoreceptor cells derived from RP iPSCs

To explore treatments that may protect rod photoreceptor cells from the accelerated cell loss induced by the *rhodopsin* mutation, we treated the cells with reagents that could modify ER stress-related pathways and quantified the Ad-p*Nrl*-EGFP-positive rod photoreceptor cells using flow cytometry after 5 weeks in differentiation culture. The reagents were added to the medium after 3 weeks of culture and were re-added each time the medium was changed (every 2–3 days). After 5 weeks of culture, the number of #5 iPSC-derived rod photoreceptor cells collected and counted by flow cytometry was significantly increased following treatment with rapamycin and PP242 (both mTOR inhibitors), AICAR (an activator of AMP kinase [AMPK]), NQDI-1 (an inhibitor of apoptosis signal-regulating kinase

1 [ASK1]), and salubrinal (an inhibitor of eukaryotic translation initiation factor 2 subunit α [eIF2α] phosphatase and protein synthesis) (Figure 4A). These data showed that the E181K mutant rhodopsin-related cell loss could be suppressed by mTOR inhibition, AMPK activation, ASK1 inhibition, or the suppression of protein synthesis.

Effect of treatments on ER stress and apoptosis markers

Next, we investigated the effects of reagents on ER stress markers in the #5 iPSC-derived rod photoreceptor cells. After the Ad-p*Nrl*-EGFP-positive cells were purified and treated with the above-mentioned reagents, mRNA was harvested from the cells and analyzed using real-time PCR. The mRNA levels of BiP and CHOP were found to be reduced following rapamycin, PP242, AICAR, NQDI-1, or salubrinal treatment (Figure 4B, C) in the Ad-p*Nrl*-EGFP-positive rod photoreceptor cells, suggesting that these reagents suppressed the ER stress caused by the mutant rhodopsin. Additionally, the expression levels of apoptosis-related molecules, which were upregulated in the rod photoreceptor cells expressing the mutant rhodopsin, were decreased following the addition of these same drugs (Figure 4D, E).

Involvement of autophagy

As ER stress is known to activate autophagy to overcome cellular dysfunction, we examined autophagy markers in each line of iPSC-derived rod photoreceptor cells in the presence and absence of treatment with different drugs. We first examined LC3 immunostaining that indicates a putative autophagosome in p*Nrl*-EGFP-positive photoreceptor cells (Figure 5A-L), and found that the presence of LC3 was obvious in the cells with *rhodopsin* mutation (Figure 5D-I), but hardly detected in the cells without the mutation (Figure 5A-C, J-L). The autophagy markers LC3, Atg5, and Atg7 were all suppressed in the #5Rw and B7 iPSC-derived rod photoreceptor cells compared to the levels in the #5 and B7Rm iPSC-derived cells (Figure 5M-O). Treatment of the #5 iPSC-derived rod photoreceptor cells with each of the reagents described above also resulted in the reduced expression of the autophagy markers LC3, ATG5, and ATG7 (Figure 5P-R).

Discussion

We generated an iPSC line from the somatic cells of a patient with RP who carried the *rhodopsin* E181K mutation, and this iPSC line was used to derive rod photoreceptor cells that harbored the same *rhodopsin* mutation. These cells were then used to demonstrate that the E181K mutation was indeed a pathogenic, disease-causing mutation and were used to explore the underlying molecular mechanisms and potential therapeutic approaches.

A considerable number of genetic abnormalities are recognized as the cause of RP pathogenesis. Although multiple genes and multiple mutations within these genes have been linked to RP, some of these mutations may, in fact, be non-pathogenic, and, in some cases, patients may have more than one mutation in their genome [1]. Moreover, RP is exceptionally heterogeneous, and the same mutation in different individuals may produce different clinical consequences due, in part, to the different genetic backgrounds of the individuals [1]. Given these complications, it has been challenging to determine the precise genotype-phenotype association of a large number of mutations. In the present study, using human iPSCs and gene manipulation, we demonstrated that the correction of a *rhodopsin* gene mutation reversed photoreceptor cell loss in the iPSC-derived rod photoreceptor cells of an RP patient, whereas mutagenesis of the *rhodopsin* gene in control iPSCs increased cell loss. These experiments directly demonstrated the pathogenicity of the *rhodopsin* mutation in an *in vitro* system. When utilizing iPSCs to analyze disease pathogenesis, there may be a concern that the observed phenotype might be related to differences in the cell lines

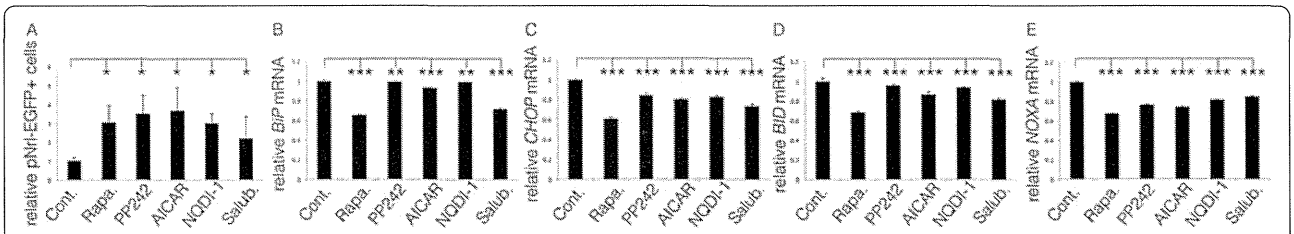

Figure 4 Drug screening in the RP #5 iPSC-derived rod photoreceptor cells. (A) Relative number of p*Nrl*-EGFP-positive rod photoreceptor cells derived from #5 iPSCs after treatment with each therapeutic reagent. N = 9. **(B-E)** Relative mRNA levels of BiP **(B)**, CHOP **(C)**, BID **(D)**, and NOXA **(E)** in the p*Nrl*-EGFP-positive cells cultured with rapamycin, PP242, AICAR, NQDI-1, and salubrinal at 5 weeks after differentiation. Each reagent increased the rod photoreceptor cell survival at 5 weeks, whereas ER stress and apoptotic markers were suppressed. N = 3 for **B-E**. Rapa., rapamycin; Salub., salubrinal. *p < 0.05, **p < 0.01, ***p < 0.001. Mean ± SD relative to cont. (with each p-values of marked by *) for Cont., Rapa., PP242, AICAR, NQDI-1, Salbr. in **(A)** 1 ± 0.182, 3.02 ± 0.920, 3.49 ± 0.976, 3.67 ± 1.22, 2.99 ± 0.513, 2.19 ± 1.12 (all, p < 0.0001); **(B)** 1 ± 0.005, 0.654 ± 0.001, 0.990 ± 0.001, 0.932 ± 0.001, 0.989 ± 0.001, 0.714 ± 0.004 (all, p < 0.0001); **(C)** 1 ± 0.002, 0.608 ± 0.003, 0.842 ± 0.009, 0.802 ± 0.003, 0.830 ± 0.003, 0.733 ± 0.008 (all, p < 0.0001); **(D)** 1 ± 0.016, 0.681 ± 0.006, 0.954 ± 0.007, 0.864 ± 0.002, 0.934 ± 0.004, 0.816 ± 0.008 (all, p < 0.0001); **(E)** 1 ± 0.005, 0.671 ± 0.001, 0.760 ± 0.004, 0.743 ± 0.003, 0.816 ± 0.001, 0.849 ± 0.006 (all, p < 0.0001). These data were obtained by technical triplicate and not by biological triplicate. All statistical analyses in this figure were carried out by One-way ANOVA Dunnett's test.

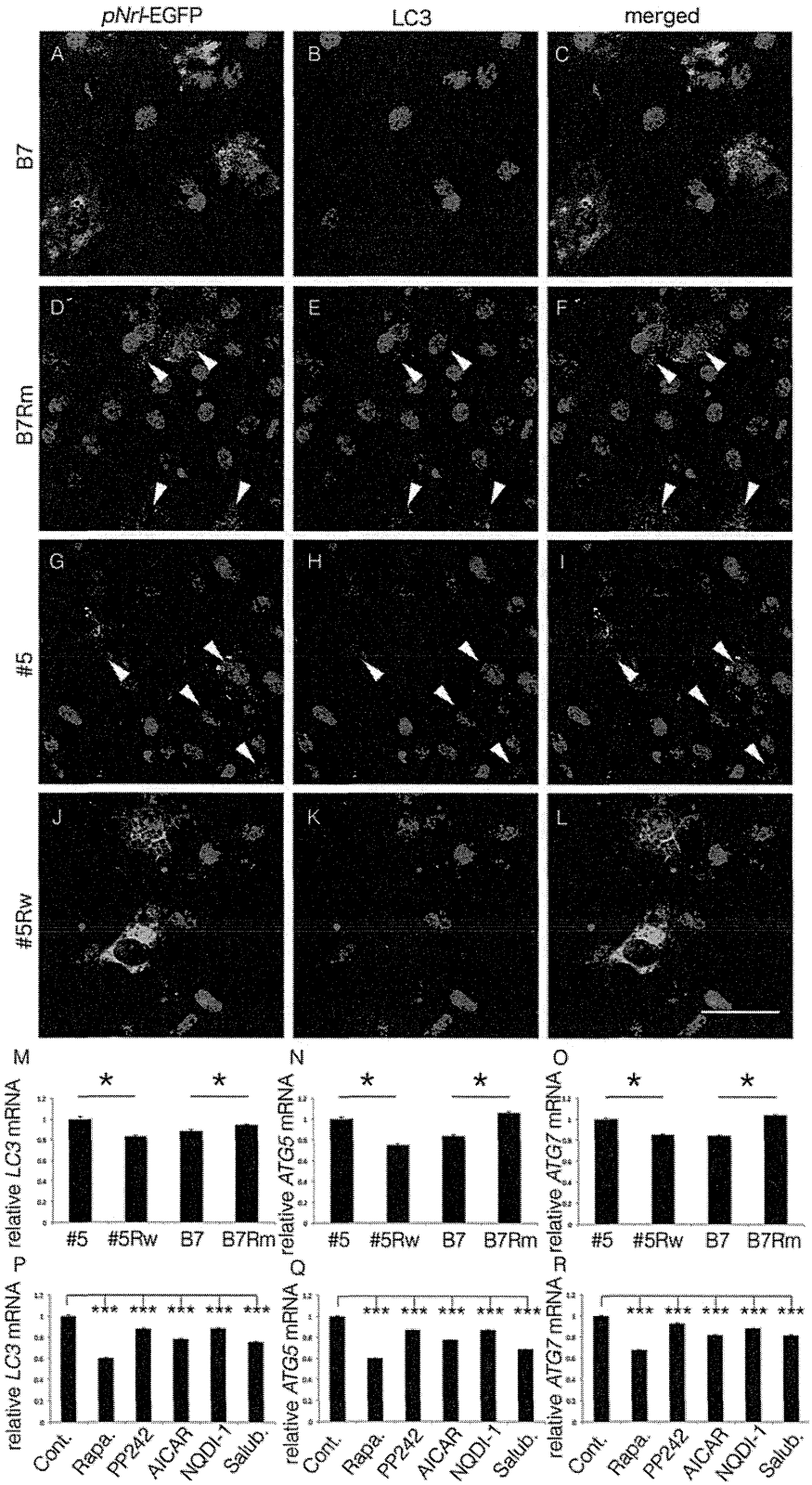

Figure 5 (See legend on next page.)

(See figure on previous page.)
Figure 5 Autophagy markers in iPSC-derived rod photoreceptor cells. Immunostaining of p*Nrl*-EGFP-positive cells (green: **A**, **D**, **G** and **J**) and immunocytochemistry using anti-LC3 antibody (magenta: **B**, **E**, **H** and **K**), and their merged images (**C, F, I, L**). Arrowheads indicated p*Nrl*-EGFP- and LC3-double positive cells. Scale bar: 20 μm. The autophagy marker molecules LC3 (**M, P**), ATG5 (**N, Q**), and ATG7 (**O, R**) were analyzed using real-time PCR in the p*Nrl*-EGFP-positive rod photoreceptor cells derived from each iPSC line in the absence of treatment (**M-O**) and in #5 iPSC-derived cells following therapeutic treatment (**P-R**), both at 5 weeks of culture. Autophagy was suppressed in the #5Rw and B7 iPSC-derived cells and in the #5 iPSC-derived cells with each treatment. N = 3 for all. Rapa., rapamycin; Salub., salubrinal. *$p < 0.05$, ***$p < 0.001$. Mean ± SD (with each p-values of marked by *) for #5, #5Rw, B7, B7#Rm in **(M)** 1 ± 0.010, 0.830 ± 0.005 ($p < 0.0001$), 0.881 ± 0.008, 0.943 ± 0.003 ($p = 0.002$); **(N)** 1 ± 0.007, 0.747 ± 0.005 ($p < 0.0001$), 0.836 ± 0.005, 1.06 ± 0.006 ($p < 0.0001$); **(O)** 1 ± 0.004, 0.849 ± 0.003 ($p < 0.0001$), 0.842 ± 0.003, 1.04 ± 0.003 ($p < 0.0001$). Mean ± SD relative to cont. (with each p-values of marked by *), for Cont., Rapa., PP242, AICAR, NQDI-1, Salbr. for **(P)** 1 ± 0.010, 0.601 ± 0.001, 0.873 ± 0.011, 0.784 ± 0.004, 0.885 ± 0.004, 0.757 ± 0.002 (all, $p < 0.0001$); **(Q)** 1 ± 0.007, 0.599 ± 0.001, 0.867 ± 0.004, 0.772 ± 0.003, 0.872 ± 0.0003, 0.683 ± 0.001 (all, $p < 0.0001$); **(R)** 1 ± 0.004, 0.675 ± 0.001, 0.924 ± 0.003, 0.818 ± 0.002, 0.879 ± 0.001, 0.818 ± 0.004 (all, $p < 0.0001$). These data were obtained by technical triplicate and not by biological triplicate. Statistical analyses in **M-O** and **P-R** were carried out by Student's T test and by One-way ANOVA Dunnett's test, respectively.

that reflect differences in the reprogramming process [22]. Thus, to exclude such a concern, we investigated the effect of correcting the genetic defect in the patient-derived iPSC line, aiming to clarify the genotype-phenotype causal relationship.

This genetically well-controlled study was facilitated by the use of HDAdV for the gene targeting of human iPSCs. HDAdV was originally developed to overcome host immune responses to E1-deleted AdV, the adenovirus commonly used for gene transfer [23]. Because the viral genes are completely removed from the vector genome, the HDAdV system is less toxic to the infected cells. Moreover, the increased cloning capacity of HDAdV when combined with negative selection was shown to result in an increased frequency of targeted integrations in human iPSCs [24]. In the present study, the use of this methodology resulted in the successful generation of targeted iPSCs, and large gene targeting in iPSCs will be useful for establishing the pathogenesis of various candidate genes associated with hereditary diseases [25]. Moreover, because HDAdV gene transfer does not result in the transfer of viral sequences, this technique may also have the potential to be used for gene therapy via iPSC transplantation. Indeed, the HDAdV gene transfer system has several advantages compared to other genome-editing methods, such as CRISPR (clustered regularly interspaced short palindromic repeats) or TALEN (Transcription Activator-Like Effector Nucleases), which may induce off-target alterations [26]. Fu et al. reported that the off-target sites caused by CRISPR harbored up to five mismatches, and many sites were mutagenized with frequencies comparable to those observed at the intended on-target site. This is because the DNA break caused by Cas9 nuclease, which leads to the genome editing, can be guided by simple base-pair complementarity between the first 20 nucleotides of an engineered guide RNA-target DNA interface and can be easily misguided by sensing mismatched sequences. Undesired off-target sites when using TALEN are also related to unintended DNA cleavage [27]. In contrast, the HDAdV gene transfer system does not require DNA cleavage but instead requires homologous recombination; therefore, this technique results in few off-target effects.

Clinical trials using several therapeutic approaches for RP are currently in progress. One example is retinal pigment epithelium-specific 65-kDa protein (*RPE65*) gene therapy for the treatment of Leber's congenital amaurosis (LCA); this autosomal recessive abnormality is caused by a loss-of-function of RPE65 and can thus be treated through the introduction of the normal gene.

In contrast, a different approach is required for autosomal dominant diseases caused by mutations that result in a toxic gain-of-function protein. A randomized trial of ciliary neurotrophic factor (CNTF) was performed to evaluate the safety and efficacy of this factor with regard to the visual functions of RP patients [28]. Although this treatment caused no serious adverse events, retinal sensitivity was reduced, possibly due to rhodopsin degradation [29] in response to CNTF. Thus, definitive therapeutic approaches for RP have not yet been established. Our study using a patient's iPSC-derived photoreceptor cells offers a novel approach for the evaluation of potential of new therapeutics.

We found that treatment with salubrinal, a selective inhibitor of eIF2α, led to an increased number of #5 iPSC-derived rod photoreceptor cells. Additionally, the treated cells showed reduced levels of ER stress and apoptotic markers, suggesting that the rod photoreceptor cell death caused by the *rhodopsin* E181K mutation could be suppressed by inhibiting protein synthesis, including the synthesis of the abnormal rhodopsin. Treatment with NQDI-1, an inhibitor of ASK1 activation, also increased the survival of the mutant rod photoreceptor cells, consistent with the idea that apoptosis is regulated by the ER stress-induced Ire-1α-ASK1-JNK pathway [30,31].

Based on these findings, we further investigated the ER stress-induced apoptosis pathway using additional reagents that modify this signaling pathway. Treatment with rapamycin reduced ER stress markers in the #5 iPSC-derived rod photoreceptor cells and significantly

increased cell survival. The accumulation of unfolded mutant rhodopsin protein, which increases ER stress, may have activated the mTORC1-regulated Ire1α-ASK1-JNK apoptotic pathway [30]; mTORC1 can further increase cell death through a positive feedback mechanism, resulting in increased protein synthesis, including the mutated rhodopsin [30]. Thus, the protective effect of rapamycin in these cells may be due to the suppression of the vicious cycle between the UPR (unfolded protein response) and mTORC1 pathways. This FDA-approved drug (rapamycin) can be reassessed to treat RP; however, further studies are required. In contrast to rapamycin, PP242 inhibits both mTORC1 and mTORC2; the latter is also influenced by UPR, and mTORC2 signaling induces survival signaling via AKT activation [30]. This contradictory action of mTORC2 may limit the overall effect of PP242 on the suppression of cell death.

AMPK activation through AICAR treatment also exhibited a protective effect by reducing ER stress and increasing photoreceptor cell survival. Previous studies have shown that AMPK suppresses mTORC1 indirectly through the phosphorylation and activation of the tuberous sclerosis complex (TSC) [30,32]. Additionally, extensive studies have also revealed that the activity of mTORC1 is modulated by intracellular energy levels through multiple mechanisms, and AMPK is reported to directly phosphorylate multiple components of the mTORC1 pathway [32].

Autophagy is a process that involves the degradation of proteins and organelles in response to various forms of cellular stress, including ER stress [14]. The unfolded or misfolded proteins in the ER lumen that cause ER stress are translocated to the cytoplasm where they are degraded. During this process, the ubiquitin proteasome system and autophagy act as degradation systems for the unfolded proteins. Thus, disturbing autophagy renders the cells vulnerable to ER stress, as autophagy plays important roles in cell survival after ER stress [15]. The absence of autophagy may cause neurodegenerative diseases [33,34], and autophagy has also been shown to cause apoptosis in some diseases by destroying cellular components [35]. Accordingly, we examined the expression of autophagy markers in the iPSC-derived rod photoreceptor cells with or without the *rhodopsin* mutation. We found that the levels of autophagy markers changed in parallel with the levels of ER stress and the levels of the apoptosis markers. We interpret this result that the decrease in autophagy markers following the drug treatments may have resulted from the decreased demand for autophagy following the suppression of ER stress.

In the present study, to examine the effects of various drugs, and characterize the ER stress and autophagy marker expression, we could obtain consistent results with low p-values in the triplicated real-time PCR experiment (Figures 4 and 5). Strictly, however, these results can be interpreted as follows. Because of the limitation of the culture scale, we had to put each iPSC-derived p*NrL*-GFP positive rod photoreceptor cells which were obtained from each culture well together, before reverse transcription. Thus, each real-time PCR data in Figures 4 and 5 was obtained using the same RT-product as a template, rather than biological triplicate. These experimental conditions can explain why such low p-values for the mRNA expression changes by various drugs' treatment. Thus, in the future investigations, these results should be re-confirmed using biological triplicate by performing larger scale of iPSC cultures and subsequent photoreceptor differentiation assays.

To obtain target cells that could be used to explore different therapeutic approaches, we used Lamba's differentiation method [16], which allows the cells to express rod photoreceptor cell markers within only a few weeks. Considering that the human photoreceptor require more time to mature *in vivo*, it is possible that the photoreceptor cells derived using this method have artificial intracellular microenvironments. In fact, there are several protocols for retinal differentiation that involve months of culture [11,12,36,37]. However, the method used in the present study required less time and constitutes an efficient strategy for creating cells that can be used to examine pathogenic genes and screen novel therapeutics, which can be then applied in industrial uses.

Conclusions

In summary, the generation of iPSCs from an RP patient was a valuable approach to demonstrate a causative link between a pathogenic mutation and a cellular phenotype. The use of iPSCs derived from RP and control individuals, combined with the manipulations of the gene of interest using HDAdV, allowed us to examine the effects of normal and mutant rhodopsin in otherwise genetically identical rod photoreceptor cells. Further studies using similar systems should help to reveal the molecular mechanisms underlying other genetic diseases and could serve as a cellular platform for the evaluation of potential therapeutics, including the large-scale screening of compound libraries.

Methods

This study followed the tenets of the Declaration of Helsinki and was approved by the ethics committee at Keio University School of Medicine (Approval No. 2008016).

Isolation of human skin cells and generation of iPSCs

Skin cells were obtained from a 53-year-old Japanese female RP patient by a skin-punch biopsy after the patient gave her written, informed consent. These cells were then infected with retroviruses encoding four reprogramming

factors, Oct3/4, Sox2, Klf4, and c-Myc, as previously described, to generate a human iPSC line, RP#5 (#5), [15,38]. The control iPSC line [201B7 (B7)], which was generated using the same method described for #5, was kindly provided by Dr. Shinya Yamanaka of Kyoto University [15]. The sequences of the *rhodopsin* genes in the iPSCs (see Additional file 1: Table S1) and the immunostaining of pluripotent markers (see Additional file 2: Table S2) were analyzed; teratoma formation was confirmed as previously described [38].

Preparation of HDAdVs and gene targeting

HDAdVs were prepared as previously described to generate gene-targeted iPSCs (#5Rw and B7Rm clones) (see Results and Additional file 3).

Differentiation, collection, and analyses of rod photoreceptor cells

The *in vitro* differentiation of the rod photoreceptor cells from iPSCs was performed as previously reported (see Additional file 3) [16]. The differentiated cells were infected with Ad-p*Nrl*-EGFP, which was generated using the pENTR1A plasmid harboring the *Nrl* promoter region (kindly provided by Dr. Anand Swaroop, NIH, MD) [19], 2 days prior to each analysis. The cells were suspended in PBS containing 10 μg/ml propidium iodide (PI) to stain the non-viable cells and were sorted to collect the EGFP-positive viable cells using a triple-laser MoFlo (Dako), FACS Calibur or FACS Aria (BD Biosciences) flow cytometer. The collected cells were counted or used for a real-time PCR analysis (see Additional file 1: Table S1). For real-time PCR analyses, the differentiated cells were summed up from each culture well according to the iPSC groups or the treatment groups. Annexin V staining was performed using Annesin V-Biotin Apoptosis Detection Kit (Bio Vision), followed by the staining with Streptoavidin, Allophcocyanin, crosslinked, conjugated antibody (Life Technoloties). Immunohistochemical analyses were performed using antibodies listed in Additional file 2: Table S2. Images were obtained using LSM-710 confocal (Zeiss) microscopes.

Treatment protocol

The iPSC-derived cells were treated with the following drugs after 3 weeks of differentiation: 10 nM rapamycin (Selleckchem.com), 500 nM PP242 (Sigma-Aldrich), 2 μM 5-aminoimidazole-4-carboxyamide ribonucleoside (AICAR, Santa Cruz), 500 nM Nuclear Quality Assurance-1 (NQDI-1, Axon Medchem), and 3 μM salubrinal (Millipore).

Statistical analyses

All the results are expressed as the mean ± SD. The differences were analyzed using the Student's T test (between 2 groups) and Dunnett's test (among 6 groups), and the differences were considered significant when $p < 0.05$. All statistical tests were performed using IBM SPSS statistics Ver.19 (IBM, Armonk, NY) and confirmed using Stata13 (Light Stone, Tokyo, Japan).

Additional files

Additional file 1: Table S1. Primer list.

Additional file 2: Table S2. Antibody list.

Additional file 3: Supplementary materials and methods.

Competing interests

H. Okano is the scientific consultant of San Bio, Inc; Eisai Co Ltd; and Daiichi Sankyo Co Ltd.

Authors' contributions

TY, YO, SS, KT, and HO conceived and designed the experiments. TY performed most of the experiments, analyzed the data, and wrote the manuscript. YO and HO edited the manuscript. YO, WA, and MO generated the patient-derived iPSCs. KS and KM generated the genetically modified iPSCs. KY performed the statistical analyses and some of the *in vitro* culture assays. YM performed the flow cytometric analyses. All the authors read and approved the final manuscript.

Acknowledgements

We are grateful to Dr. Shinya Yamanaka (Kyoto University) for the 201B7 iPSCs and Dr. Yohei Okada for technical guidance and supervision. We would like to thank Dr. Yoichi Imaizumi, Dr. Tetsuro Kobayashi, Ms. Yuka Hirabayashi, Mr. Sadafumi Suzuki, and Ms. Haruna Koizumi-Mabuchi for their technical assistance. This work was supported by the Project for the Realization of Regenerative Medicine and Support for the Core Institute for iPS Cell Research from the Japanese Ministry of Education, Culture, Sports, Science and Technology (MEXT) to HO, a Grant-in-aid from the Global COE Program at Keio University, JSPS KAKENHI to YO (24592647) and TY (23592616), and a Grant-in-aid from the Keio Gijuku Fukuzawa Memorial Fund for the Advancement of Education and Research to YO.

Author details

[1]Laboratory of Retinal Cell Biology, Department of Ophthalmology, Keio University School of Medicine, 35 Shinanomachi, Shinjuku-ku 160-8582, Tokyo, Japan. [2]Department of Ophthalmology, Keio University School of Medicine, 35 Shinanomachi, Shinjuku-ku, Tokyo 160-8582, Japan. [3]Division of Gene Therapy, Research Center of Genome Medicine, Saitama Medical University, 1397-1 Yamane, Hidaka-shi, Saitama 350-1241, Japan. [4]Department of Dermatology, Keio University School of Medicine, 35 Shinanomachi, Shinjuku-ku 160-8582 Tokyo, Japan. [5]Department of Physiology, Keio University School of Medicine, 35 Shinanomachi, Shinjuku-ku 160-8582, Tokyo, Japan.

Received: 19 November 2013 Accepted: 28 May 2014
Published: 16 June 2014

References

1. Daiger SP, Sullivan LS, Bowne SJ: **Genes and mutations causing retinitis pigmentosa.** *Clin Genet* 2013, **84**:132–141.
2. Kaushal S: **Effect of rapamycin on the fate of P23H opsin associated with retinitis pigmentosa.** *Trans Am Ophthalmol Soc* 2006, **104**:517–529.
3. Mendes HF, van der Spuy J, Chapple JP, Cheetham ME: **Mechanisms of cell death in rhodopsin retinitis pigmentosa: implications for therapy.** *Trends Mol Med* 2005, **11**:177–185.
4. Griciuc A, Aron L, Ueffing M: **ER stress in retinal degeneration: a target for rational therapy?** *Trends Mol Med* 2011, **17**:442–451.
5. Fribley A, Zhang K, Kaufman RJ: **Regulation of apoptosis by the unfolded protein response.** *Methods Mol Biol* 2009, **559**:191–204.
6. Griciuc A, Aron L, Ueffing M: **Looking into eyes: rhodopsin pathologies in Drosophila.** *Adv Exp Med Biol* 2012, **723**:415–423.
7. Gorbatyuk MS, Knox T, LaVail MM, Gorbatyuk OS, Noorwez SM, Hauswirth WW, Lin JH, Muzyczka N, Lewin AS: **Restoration of visual function in P23H**

rhodopsin transgenic rats by gene delivery of BiP/Grp78. *Proc Natl Acad Sci U S A* 2010, **107**:5961–5966.
8. Sakami S, Maeda T, Bereta G, Okano K, Golczak M, Sumaroka A, Roman AJ, Cideciyan AV, Jacobson SG, Palczewski K: **Probing mechanisms of photoreceptor degeneration in a new mouse model of the common form of autosomal dominant retinitis pigmentosa due to P23H opsin mutations.** *J Biol Chem* 2011, **286**:10551–10567.
9. Ito D, Okano H, Suzuki N: **Accelerating progress in induced pluripotent stem cell research for neurological diseases.** *Ann Neurol* 2012, **72**:167–174.
10. Lindvall O, Barker RA, Brüstle O, Isacson O, Svendsen CN: **Clinical translation of stem cells in neurodegenerative disorders.** *Cell Stem Cell* 2012, **10**:151–155.
11. Jin ZB, Okamoto S, Osakada F, Homma K, Assawachananont J, Hirami Y, Iwata T, Takahashi M: **Modeling retinal degeneration using patient-specific induced pluripotent stem cells.** *PLoS ONE* 2011, **6**:e17084.
12. Jin ZB, Okamoto S, Xiang P, Takahashi M: **Integration-free induced pluripotent stem cells derived from retinitis pigmentosa patient for disease modeling.** *Stem Cells Transl Med* 2012, **1**:503–509.
13. Saga M, Mashima Y, Akeo K, Oguchi Y, Kudoh J, Shimizu N: **Autosomal dominant retinitis pigmentosa. A mutation in codon 181 (Glu– > Lys) of the rhodopsin gene in a Japanese family.** *Ophthalmic Genet* 1994, **15**:61–67.
14. Ogata M, Hino S, Saito A, Morikawa K, Kondo S, Kanemoto S, Murakami T, Taniguchi M, Tanii I, Yoshinaga K, Shiosaka S, Hammarback JA, Urano F, Imaizumi K: **Autophagy is activated for cell survival after endoplasmic reticulum stress.** *Mol Cell Biol* 2006, **26**:9220–9231.
15. Takahashi K, Tanabe K, Ohnuki M, Narita M, Ichisaka T, Tomoda K, Yamanaka S: **Induction of pluripotent stem cells from adult human fibroblasts by defined factors.** *Cell* 2007, **131**:861–872.
16. Lamba DA, McUsic A, Hirata RK, Wang PR, Russell D, Reh TA: **Generation, purification and transplantation of photoreceptors derived from human induced pluripotent stem cells.** *PLoS ONE* 2010, **5**:e8763.
17. Lamba DA, Karl MO, Ware CB, Reh TA: **Efficient generation of retinal progenitor cells from human embryonic stem cells.** *Proc Natl Acad Sci U S A* 2006, **103**:12769–12774.
18. Lamba DA, Gust J, Reh TA: **Transplantation of human embryonic stem cell-derived photoreceptors restores some visual function in Crx-deficient mice.** *Cell Stem Cell* 2009, **4**:73–79.
19. Akimoto M, Cheng H, Zhu D, Brzezinski JA, Khanna R, Filippova E, Oh EC, Jing Y, Linares JL, Brooks M, Zareparsi S, Mears AJ, Hero A, Glaser T, Swaroop A: **Targeting of GFP to newborn rods by Nrl promoter and temporal expression profiling of flow-sorted photoreceptors.** *Proc Natl Acad Sci U S A* 2006, **103**:3890–3895.
20. Mears AJ, Kondo M, Swain PK, Takada Y, Bush RA, Saunders TL, Sieving PA, Swaroop A: **Nrl is required for rod photoreceptor development.** *Nat Genet* 2001, **29**:447–452.
21. Swaroop A, Wang QL, Wu W, Cook J, Coats C, Xu S, Chen S, Zack DJ, Sieving PA: **Leber congenital amaurosis caused by a homozygous mutation (R90W) in the homeodomain of the retinal transcription factor CRX: direct evidence for the involvement of CRX in the development of photoreceptor function.** *Hum Mol Genet* 1999, **8**:299–305.
22. Miura K, Okada Y, Aoi T, Okada A, Takahashi K, Okita K, Nakagawa M, Koyanagi M, Tanabe K, Ohnuki M, Ogawa D, Ikeda E, Okano H, Yamanaka S: **Variation in the safety of induced pluripotent stem cell lines.** *Nat Biotechnol* 2009, **27**:743–745.
23. Suzuki K, Mitsui K, Aizawa E, Hasegawa K, Kawase E, Yamagishi T, Shimizu Y, Suemori H, Nakatsuji N, Mitani K: **Highly efficient transient gene expression and gene targeting in primate embryonic stem cells with helper-dependent adenoviral vectors.** *Proc Natl Acad Sci U S A* 2008, **105**:13781–13786.
24. Aizawa E, Hirabayashi Y, Iwanaga Y, Suzuki K, Sakurai K, Shimoji M, Aiba K, Wada T, Tooi N, Kawase E, Suemori H, Nakatsuji N, Mitani K: **Efficient and accurate homologous recombination in hESCs and hiPSCs using helper-dependent adenoviral vectors.** *Mol Ther* 2012, **20**:424–431.
25. Jiang J, Jing Y, Cost GJ, Chiang JC, Kolpa HJ, Cotton AM, Carone DM, Carone BR, Shivak DA, Guschin DY, Pearl JR, Rebar EJ, Byron M, Gregory PD, Brown CJ, Urnov FD, Hall LL, Lawrence JB: **Translating dosage compensation to trisomy 21.** *Nature* 2013, **500**:296–300.
26. Fu Y, Foden JA, Khayter C, Maeder ML, Reyon D, Joung JK, Sander JD: **High-frequency off-target mutagenesis induced by CRISPR-Cas nucleases in human cells.** *Nat Biotechnol* 2013, **31**:822–826.
27. Hockemeyer D, Wang H, Kiani S, Lai CS, Gao Q, Cassady JP, Cost GJ, Zhang L, Santiago Y, Miller JC, Zeitler B, Cherone JM, Meng X, Hinkley SJ, Rebar EJ, Gregory PD, Urnov FD, Jaenisch R: **Genetic engineering of human pluripotent cells using TALE nucleases.** *Nat Biotechnol* 2011, **29**:731–734.
28. Birch DG, Weleber RG, Duncan JL, Jaffe GJ, Tao W, Ciliary Neurotrophic Factor Retinitis Pigmentosa Study Groups: **Randomized trial of ciliary neurotrophic factor delivered by encapsulated cell intraocular implants for retinitis pigmentosa.** *Am J Ophthalmol* 2013, **156**:283–292.
29. Ozawa Y, Nakao K, Shimazaki T, Shimmura S, Kurihara T, Ishida S, Yoshimura A, Tsubota K, Okano H: **SOCS3 is required to temporally fine-tune photoreceptor cell differentiation.** *Dev Biol* 2007, **303**:591–600.
30. Appenzeller-Herzog C, Hall MN: **Bidirectional crosstalk between endoplasmic reticulum stress and mTOR signaling.** *Trends Cell Biol* 2012, **22**:274–282.
31. Nishitoh H, Matsuzawa A, Tobiume K, Saegusa K, Takeda K, Inoue K, Hori S, Kakizuka A, Ichijo H: **ASK1 is essential for endoplasmic reticulum stress-induced neuronal cell death triggered by expanded polyglutamine repeats.** *Genes Dev* 2002, **16**:1345–1355.
32. Inoki K, Ouyang H, Zhu T, Lindvall C, Wang Y, Zhang X, Yang Q, Bennett C, Harada Y, Stankunas K, Wang CY, He X, MacDougald OA, You M, Williams BO, Guan KL: **TSC2 integrates Wnt and energy signals via a coordinated phosphorylation by AMPK and GSK3 to regulate cell growth.** *Cell* 2006, **126**:955–968.
33. Chen Y, Sawada O, Kohno H, Le YZ, Subauste C, Maeda T, Maeda A: **Autophagy protects the retina from light-induced degeneration.** *J Biol Chem* 2013, **288**:7506–7518.
34. Harris H, Rubinsztein DC: **Control of autophagy as a therapy for neurodegenerative disease.** *Nat Rev Neurol* 2011, **8**:108–117.
35. Codogno P, Meijer AJ: **Autophagy and signaling: their role in cell survival and cell death.** *Cell Death Differ* 2005, **Suppl 2**:1509–1518.
36. Osakada F, Ikeda H, Mandai M, Wataya T, Watanabe K, Yoshimura N, Akaike A, Sasai Y, Takahashi M: **Toward the generation of rod and cone photoreceptors from mouse, monkey and human embryonic stem cells.** *Nat Biotechnol* 2008, **26**:215–224.
37. Meyer JS, Shearer RL, Capowski EE, Wright LS, Wallace KA, McMillan EL, Zhang SC, Gamm DM: **Modeling early retinal development with human embryonic and induced pluripotent stem cells.** *Proc Natl Acad Sci U S A* 2009, **106**:16698–16703.
38. Imaizumi Y, Okada Y, Akamatsu W, Koike M, Kuzumaki N, Hayakawa H, Nihira T, Kobayashi T, Ohyama M, Sato S, Takanashi M, Funayama M, Hirayama A, Soga T, Hishiki T, Suematsu M, Yagi T, Ito D, Kosakai A, Hayashi K, Shouji M, Nakanishi A, Suzuki N, Mizuno Y, Mizushima N, Amagai M, Uchiyama Y, Mochizuki H, Hattori N, Okano H: **Mitochondrial dysfunction associated with increased oxidative stress and α-synuclein accumulation in PARK2 iPSC-derived neurons and postmortem brain tissue.** *Mol Brain* 2012, **5**:35.

doi:10.1186/1756-6606-7-45
Cite this article as: Yoshida *et al.*: The use of induced pluripotent stem cells to reveal pathogenic gene mutations and explore treatments for retinitis pigmentosa. *Molecular Brain* 2014 **7**:45.

Biochemical and Biophysical Research Communications 447 (2014) 683–688

Contents lists available at ScienceDirect

Biochemical and Biophysical Research Communications

journal homepage: www.elsevier.com/locate/ybbrc

Differentiation, polarization, and migration of human induced pluripotent stem cell-derived neural progenitor cells co-cultured with a human glial cell line with radial glial-like characteristics

Yohei Bamba [a,b], Tomoko Shofuda [c], Daisuke Kanematsu [b], Masahiro Nonaka [d], Mami Yamasaki [e,f], Hideyuki Okano [a], Yonehiro Kanemura [b,d,*]

[a] Department of Physiology, Keio University School of Medicine, 35 Shinanomachi, Shinjuku-ku, Tokyo 160-8582, Japan
[b] Division of Regenerative Medicine, Institute for Clinical Research, Osaka National Hospital, National Hospital Organization, 2-1-14 Hoenzaka, Chuo-ku, Osaka 540-0006, Japan
[c] Division of Stem Cell Research, Institute for Clinical Research, Osaka National Hospital, National Hospital Organization, Osaka, Japan
[d] Department of Neurosurgery, Osaka National Hospital, National Hospital Organization, Osaka, Japan
[e] Department of Pediatric Neurosurgery, Takatsuki General Hospital, Takatsuki, Japan
[f] Division of Molecular Medicine, Institute for Clinical Research, Osaka National Hospital, National Hospital Organization, Osaka, Japan

ARTICLE INFO

Article history:
Received 11 April 2014
Available online 19 April 2014

Keywords:
Induced pluripotent stem cells
Glioma
Neuronal migration
Radial glia
PiggyBac transposon
Regenerative medicine

ABSTRACT

Here we established a unique human glial cell line, GDC90, derived from a human glioma and demonstrated its utility as a glial scaffold for the polarization and differentiation of human induced pluripotent stem cell-derived neural progenitor cells (iPSC-NPCs). When co-cultured with GDC90 cells, iPSC-NPCs underwent rapid polarization and neurite extension along the radially spreading processes of the GDC90 cells, and showed migratory behavior. This method is potentially useful for detailed examination of neurites or for controlling neurites behavior for regenerative medicine.

1. Introduction

During embryonic corticogenesis, neural progenitor cells (NPCs) and neuronal cells have complicated interactions with glial cells. In particular, radial glia (RG) cells construct the framework and control the alignment of neuronal cells during embryonic CNS development [1]. Glial cells are also important for the differentiation of NPCs derived from pluripotent stem cells (PSCs) and induced pluripotent stem cells (iPSCs) [2]. It is now possible to investigate developmental processes of the human central nervous system (CNS) and the pathogenesis of neural disorders using human PSCs [3–6]. iPSC-derived NPCs (iPSC-NPCs) can produce both neuronal and glial cells; however, they tend to remain neurogenic for a prolonged period [7,8]. Extensive research has led to methods for promoting iPSC differentiation toward specific lineages. However, the differentiation propensities of the iPSCs and iPSC-NPCs are not completely controlled. Furthermore, iPSC-NPCs produce neuronal cells with disordered and randomly arranged neurites, which complicates the examination of neurite morphology and dynamics. The disorderly arrangement of neurites in *in vitro* cultures may be due to the absence of the radial glial scaffold that is abundant during *in vivo* corticogenesis.

This shortage of glial scaffolds *in vitro* is addressed by co-culturing iPSC-NPCs with glial cells. Human iPSC-NPCs can be induced to develop into mature neurons by culturing them with mouse primary astrocytes [2]. However, the isolation of primary glial cells for each experiment is time-consuming and laborious. Thus, the use of a human glial cell line as a scaffold for iPSC-NPC differentiation may be a more efficient approach.

Here, we established a co-culture system using iPSC-NPCs and a unique glial cell line, GDC90, which promoted iPSC-NPC differentiation, polarization, and migration. Use of this unique human glial cell line may shed light on the detailed morphological behaviors of iPSC-NPCs and contribute to their application in regenerative medicine.

Abbreviations: iPSCs, induced pluripotent stem cells; iPSC-NPCs, iPSC-derived neural progenitor cells; RG, radial glia; PB, PiggyBac.

* Corresponding author at: Division of Regenerative Medicine, Institute for Clinical Research, Osaka National Hospital, National Hospital Organization, 2-1-14 Hoenzaka, Chuo-ku, Osaka 540-0006, Japan. Fax: +81 6 6946 3530.
E-mail address: kanemura@onh.go.jp (Y. Kanemura).

http://dx.doi.org/10.1016/j.bbrc.2014.04.070
0006-291X/

2. Materials and methods

2.1. Human tissues and cells

This study was carried out in accordance with the principles of the Helsinki Declaration, and approval for the use of human tissues and cells was obtained from the ethical committees of Osaka National Hospital and Keio University School of Medicine (Nos. 94, 110, 146, IRB0713). Surgically removed primary brain tumor tissues were collected at the Osaka National Hospital with written informed consent.

Human iPSC clone 201B7 [9], obtained from the RIKEN cell bank (Tsukuba, Japan), was propagated on Mitomycin C-treated mouse embryonic fibroblast (MEF) feeder cells as previously described [10].

Two human glioma cell lines derived from glioblastoma multiforme (GBM), U-251MG (IFO50288, The Japan Health Sciences Foundation, Tokyo, Japan) and U-87MG (HTB-14, ATCC), were propagated in culture medium with 10% fetal bovine serum. Human neural stem cells (oh-NSC-3-fb) derived from the fetal forebrain were propagated by the neurosphere method as previously described [11].

2.2. Isolation of glioma-derived cells

Glioma-derived cells (GDCs) were isolated from GBM specimens using a serum-free suspension culture method as previously described [11].

2.3. Generation of iPSC-NPCs

NPCs were generated from the human iPSC line 201B7 by embryoid body formation and subsequent neurosphere culture as previously described [8].

2.4. Genetic labeling by PiggyBac (PB) transposon-mediated gene transfer

A CAG promoter [12]-driven expression cassette and a neomycin-resistance gene cassette from pEBmulti-neo (Wako, Osaka, Japan) were cloned into pPB533A2 (System Biosciences, CA, USA), replacing components between two core insulators and the PB terminal repeat sequences. The coding sequence for EGFP or for tdTomato [from ptdTomato-N1 (Clontech, CA, USA)] was cloned downstream of the CAG promoter to construct pPB-CAG-EGFP (or -tdTomato) -Neo using restriction enzymes.

Nucleofection of GDC90 cells and iPSC-NPCs was performed as previously described [13]. Both 7.5 μg of the fluorescent protein expression vector and 2.5 μg of the PB transposase expression vector PB200A (System Biosciences) were introduced into 3–5 × 10^6 -cells. Fluorescent proteins were expressed in U-87MG and U-251MG cells by transfecting them with PB vectors using the FuGene HD Transfection Reagent (Promega, WI, USA). Geneticin (200–600 μg/ml, Life Technologies) was maintained in the medium until the second passage.

2.5. Quantitative RT-PCR

Total RNAs were isolated using the RNeasy Mini Kit (Qiagen, Venulo, Netherlands). Template cDNA samples were synthesized using the Prime Script RT Reagent kit (Takara, Shiga, Japan). Real-time quantitative PCR was performed with the PowerSYBR Green PCR Mix (Life Technologies) and the ABI7300 Real-time PCR system (Life Technologies) using gene-specific primer pairs (Supplemental Table 1). The expression value (Ct value) of each gene was normalized to that of GAPDH, and the normalized expression values were compared as previously described [10].

2.6. Immunocytochemistry and imaging analysis

GDC90 or iPSC-NPC aggregates were plated on Matrigel-GFR-(BD Biosciences, NJ, USA) coated glass chamber slides (Matsunami Glass, Osaka, Japan). The samples fixed with 4% paraformaldehyde were incubated with primary antibody overnight at 4 °C and then in secondary antibody and the DRAQ5 nuclear stain (Biostatus, Leicestershire, UK) for 1 h at room temperature. Images were acquired using LSM510 and LSM5 software (Carl Zeiss, Oberkochen, Germany).

The primary antibodies were rabbit anti-Nestin (1:500) [14], rabbit anti-glial fibrillary acidic protein (GFAP) (1:80, Sigma), mouse anti-βIII tubulin (1:500, Covance, Princeton, NJ, USA), rabbit anti-brain lipid binding protein (BLBP) (1:500, Millipore), rabbit anti-SOX2 (1:500, Chemicon), and rabbit anti-doublecortin (DCX) (1:400, Cell Signaling, Danvers, MA, USA). The secondary antibodies were goat anti-rabbit IgG Alexa Fluor® 488 (1:1000, Molecular Probes, CA, USA), goat anti-mouse IgG Alexa Fluor® 648 (1:1000, Molecular Probes), and goat anti-rabbit IgG Alexa Fluor® 648 (1:1000, Molecular Probes). Fluorescence microscopy was performed with an IX81 inverted microscope (Olympus, Tokyo, Japan). Time-lapse images were taken in a DH35i micro-incubation system with an automatic temperature controller (Warner Instruments, CT), using Lumina Vision software (Mitani, Fukui, Japan).

2.7. iPSC-NPC and GDC90 co-culture

For adjacent co-cultures, approximately 10 spheres each of GDC90 cells and iPSC-NPCs were collected and plated on Matrigel-GFR-(BD Biosciences) coated glass-bottom dishes (Matsunami Glass) in differentiation medium containing Neurobasal Medium (Life Technologies), 2% B27 supplement (Life Technologies), 2 mM L-glutamine (Life Technologies), and 1% Antibiotic-Antimycotic (Life Technologies). For adjacent co-cultures using U-87MG or U-251MG cells, aggregates were formed from 5 × 10^3 cells in low-attachment 96-well V-bottom (conical) plates (PrimeSurface, Sumitomo Bakelite, Tokyo, Japan). For mixed co-cultures, 5 × 10^3 U-87MG or U-251MG cells or 5.0 × 10^3 GDC90 cells and 5.0 × 10^3 iPSC-NPCs were seeded into a single well of a low attachment 96-well V-bottom plate one day before plating on the Matrigel-GFR-coated dishes.

2.8. Three-dimensional co-culture of iPSC-NPCs and GDC90 cells on a silicate membrane

Mixed aggregates containing 1 × 10^4 cells each of iPSC-NPCs and GDC90 cells, generated as described above, were plated on a CellBed silicate fiber membrane (Japan Vilene, Tokyo, Japan, http://www.cellbed-jp.com/). The green fluorescence of neurites extending from the EGFP-expressing iPSC-NPCs was observed with an IX81 fluorescence microscope.

2.9. Statistical analysis

All data represent the mean of values determined from three experiments. The statistical analysis of the results was performed by Welch's *t*-test.

3. Results

3.1. Isolation and establishment of fluorescently labeled human GDCs

We isolated a cell line, GDC90, from the tumor specimen of a 74-year-old female glioblastoma multiforme (GBM) patient. To

distinguish GDC90 cells from host or co-cultured cells, we used the PB transposon vector which contains a tdTomato-expressing cassette driven by the CAG promoter, a neomycin-resistance gene cassette, and the PB terminal repeats sequence (Fig. 1A). Following nucleofection of this vector and neomycin selection, GDC90 cells were isolated that stably expressed tdTomato and maintained fluorescence for over 10 passages, even when antibiotic selection was discontinued (Fig. 1B, C). Glioma cell lines (U-87MG, U-251MG), and GDC40 cells, another GDC line isolated from a GBM patient (Okada et al., submitted), were also labeled using the same system (Fig. 1D–I). To observe the dynamic behavior of iPSC-NPCs, we established EGFP-labeled iPSC-NPC cell lines using the same nucleofection method (Fig. 1J, K).

To characterize the glial cell lines, we examined neural marker expression using quantitative RT-PCR and immunocytochemistry. Quantitative RT-PCR (Fig. 1Q) showed that the Nestin mRNA level was higher in GDC90 than in the other glial cell lines ($n = 3$, $P < 0.001$) and that GFAP was more highly expressed in GDC90 and U-251MG cells than in iPSC-NPCs ($n = 3$, $P < 0.001$). The BLBP expression was higher in GDC90 and GDC40 than in U-251MG cells ($n = 3$, $P < 0.001$, $P < 0.01$, respectively), where high BLBP expression was previously reported [15]. The PAX6 expression was higher in GDC90 than GDC40 cells ($n = 3$, $P < 0.01$), but lower than in iPSC-NPCs ($n = 3$, $P < 0.01$). Immunocytochemical analyses showed that plated GDC90 cells had a polarized morphology with extended processes that were Nestin-, GFAP-, and BLBP-positive (Fig. 1L–N), and SOX2-positive nuclei (Fig. 1O).

Collectively, these results showed that GDC90 cells exhibited a molecular expression profile that was characteristic of both glial and NPCs. This profile may be reminiscent of RG cells, which are one of the candidate originators of human gliomas.

3.2. iPSC-NPC and glial cell co-culture system

To assess the behavior of iPSC-NPCs in contact with glial cell lines, we performed two different co-culture experiments. In the first, we plated a fluorescently labeled glial cell line (U-251MG, U-87MG, or GDC90) and iPSC-NPC spheres on the same dish (Fig. 2A). GDC90 aggregates plated on the dish extended their tdTomato-positive fibers in a regular and radial manner, and the neighboring iPSC-NPCs extended their EGFP-positive fibers along the GDC90 radial fibers (Fig. 2B). Most of the iPSC-NPC processes extended into the core of the adjacent GDC90 aggregate (Fig. 2C), and some of them even passed through the core and exited along the radial fiber on the other side (Supplementary Movie 1). In contrast to GDC90, U-251MG (Fig. 2D) and U-87MG (Fig. 2E) processes did not spread radially from the aggregates, and neighboring iPSC-NPCs did not extend their processes in a regular and radial manner in the co-culture.

In the second experiment, we generated mixed aggregates from fluorescently labeled glial cells and iPSC-NPCs (Fig. 2F). Soon after plating, numerous iPSC-NPCs had migrated out from the sphere along the radial fibers of GDC90 cells (Fig. 2G, H). Approximately 10 days after plating, we observed the translocation-like migration of iPSC-NPC-derived neurons along the radial fibers of GDC90 cells (Supplementary Movie 2). The U-251MG and U-87MG lines did not exhibit these scaffolding properties, possibly because they were isolated and cultured as adherent cells in serum-containing medium, rather than as floating neurospheres in serum-free medium. We therefore tested another human glioma-derived cell line, GDC40, which was isolated using the serum-free neurosphere method. Interestingly, although the GDC40 cells expressed radial glial marker BLBP and Nestin, similar to GDC90 cells (Fig. 1Q), they did not efficiently support iPSC-NPC neurites extension (Fig. 2I, J).

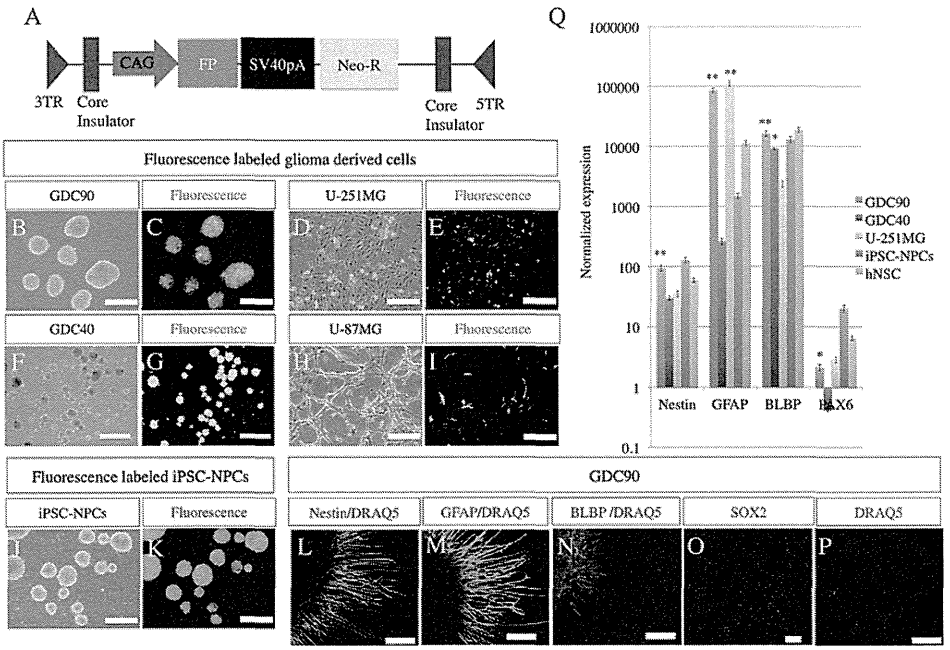

Fig. 1. Generation of fluorescently labeled cells and molecular characterization of GDC90 cells. (A) Construction of the PiggyBac transposon fluorescent protein (FP) expression vector. The CAG promoter enables strong expression in NPCs, and fluorescently labeled cells can be selected by neomycin resistance. (B–K) Proliferating GDC90 aggregates, other glial cell lines, and iPSC-NPC neurospheres with stable and strong fluorescent protein expression. Scale bar: 200 μm. (L–P) Immunocytochemistry of GDC90. GDC90 cells expressed the neural stem/progenitor cell markers Nestin and SOX2 and the RG cell markers GFAP and BLBP. Scale bar: 50 μm. (J–L): Quantitative RT-PCR analysis of GDC90. GDC90 cells expressed Nestin and GFAP and higher levels of BLBP than U-251MG cells (**$P < 0.001$, *$P < 0.01$).

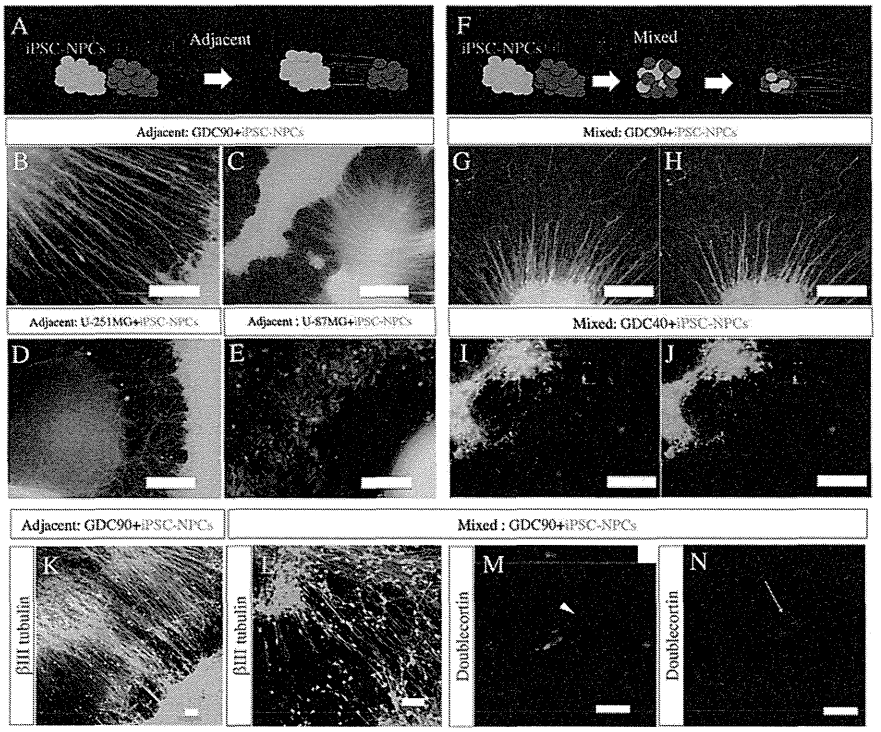

Fig. 2. Fluorescence imaging of co-cultured iPSC-NPCs and GDC90 cells. (A) Schematic of the adjacent co-culture system. iPSC-NPC neurospheres and glial aggregates were plated in contact on the same dish. Glial cells and iPSC-NPCs were distinguished by their expression of tdTomato and EGFP, respectively. (B, C) Numerous iPSC-NPC-derived neurites were observed extending along GDC90 fibers, toward GDC90 aggregates. Scale bars: 500 and 200 μm in B and C, respectively. (D, E) The other glioma cell lines, U-251MG and U-87MG, did not form polarized fibers and attracted fewer neurites. Scale bar: 200 μm. (F) Schematic of mixed co-culture system. Aggregates containing both glial cells and iPSC-NPCs were plated. (G, H) GDC90-derived polarized radial fibers spread from the mixed aggregates. iPSC-NPCs-derived neurites were spread along GDC90 radiating fibers. The neurites ran efferently from the GDC90 cells. Scale bar: 200 μm. (I, J) Cells of the other glioma-derived cell line GDC40 were not polarized and showed random fiber spreading. The co-cultured iPSC-NPCs did not become polarized and did not exhibit regular neurite extension. (K, L) Immunocytochemistry of a neuronal marker in iPSC-NPCs. In both the adjacent and mixed co-cultures, βIII tubulin-positive (blue) neurites extended radially and exhibited EGFP fluorescence. The iPSC-NPC-derived neuronal cell bodies (arrow) were migrating away from the aggregates. Scale bar: 50 μm. (M, N) Immunocytochemistry of DCX, a marker of migrating young neurons. A migrating EGFP-positive iPSC-NPC-derived neuron expressed DCX in its leading process (arrowhead). Another DCX-positive neuron labeled with EGFP fluorescence was observed migrating along a GDC90 radial fiber that was identified by its tdTomato fluorescence (arrow). Scale bar: 50 μm.

Immunocytochemical analyses of the iPSC-NPC-GDC90 co-culture showed that the EGFP-positive fibers extending from the iPSC-NPCs were βIII tubulin-positive neurites (Fig. 2K, L), which also expressed DCX, a characteristic of migrating neurons (Fig. 2M). DCX-positive iPSC-NPC-derived neurons were observed in association with tdTomato-positive glial fibers (Fig. 2N), suggesting that the GD90-co-cultured iPSC-NPCs became polarized and migrated along GDC90 processes, similar to their movement along glial scaffolds *in vivo*.

In both cultures, the iPSC-NPCs differentiated into neurons that migrated along GDC90-derived radial fibers, which supported both afferent and efferent neurite extension. Thus, GDC90 represents a unique glial cell line that supports iPSC-NPC differentiation, polarization, and migration.

3.3. Glioma-derived glial cells exhibit a strong affinity for iPSC-NPCs

In the co-culture system, iPSC-NPCs showed different responses to monolayer-cultured glioma-derived cells (U-251MG and U-87MG) versus neurosphere-cultured-GDCs (GDC90). We considered that the differently prepared GDCs might have different affinities for iPSC-NPCs. To explore this possibility, we generated mixed aggregates that contained equal numbers of glioma-derived cells and iPSC-NPCs. As expected, the GDC90 cells and iPSC-NPCs formed single aggregates, in which iPSC-NPCs were relatively abundant in the inner portion (Fig. 3D). In contrast, iPSC-NPCs and U-251MG or U-87MG failed to form homogeneous aggregates (Fig. 3E, F). Unexpectedly, the iPSC-NPCs formed patchy clusters in these aggregates after one day of culture, and the two cell types formed completely separate aggregates after five days (Fig. 3H, I). These observations indicated that GDC90 cells might have a higher affinity for iPSC-NPCs than do U-251MG or U-87MG cells. This may be partly due to differences in cell adhesion molecule expression. In fact, quantitative RT-PCR showed that the N-cadherin expression was similar in GCD90 cells and iPSC-NPCs ($P = 0.3$), but approximately half that level in U-251MG cells ($P < 0.01$) (Fig. 3J). Thus, the high affinity of GDC90 and iPSC-NPCs for each other might reflect their shared expression of N-cadherin, which is abundant in neural tissue.

3.4. GDC90 and iPSC-NPC co-culture on an artificial membrane

RG cells provide a structural framework for embryonic corticogenesis and are necessary for CNS regeneration in lower animals. Thus, we further explored the effects of GDC90 cells on iPSC-NPC behavior. To induce neurite extension three-dimensionally from iPSC-NPCs, we plated mixed GDC90 and iPSC-NPC aggregates on a silicate fiber substrate. In these membranes, large slits between the silicate fibers represent sites where GDC90 cells and iPSC-NPCs can interact directly. When these cell types were co-cultured on the artificial substrate, GDC90 cells spread across the surface of

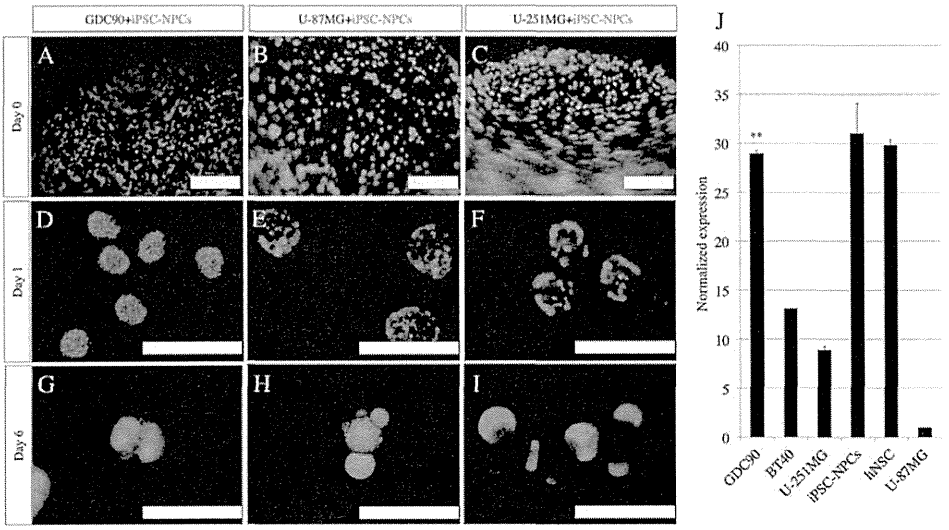

Fig. 3. GDC90 cells exhibit a higher affinity for iPSC-NPCs than do other glioma-derived cells. (A–C) Fluorescence imaging of iPSC-NPCs and glioma-derived cells just after forming mixed aggregates in V-bottom plates. (D–I) Glioma-derived cells exhibited different affinities for iPSC-NPCs. On day 1 (D–F), iPSC-NPCs formed patchy aggregates with U-251 or U-87MG cells. By day 6 the iPSC-NPCs were excluded from the U-251 or U-87 MB aggregates, while iPSC-NPCs remained in the mixed aggregates with GDC90 cells, suggesting that GDC90 cells have a higher affinity for iPSC-NPCs than do other established glioma cell lines. Scale bar: 1 mm. (J) Quantitative RT-PCR analysis of N-cadherin. N-cadherin expression levels were normalized to that of the U-87MG glioma cell line. N-cadherin expression in GDC90 cells was at least twice that in other glioma cells lines (**$P < 0.001$). iPSC-NPCs expressed high levels of N-cadherin, similar to that of the human neural stem cell line (hNSC).

the membrane, and their outgrowth led to scaffold formation, followed by iPSC-NPC-derived neurite extension (Fig. 4A–C). Even after two months of culture, the iPSC-NPC-derived neurons survived on the membrane; they exhibited a highly polarized morphology, characterized by the extension of long neurites (Fig. 4D–F). Based on these observations, we concluded that GDC90 cells could be used in conjunction with the artificial substrate as a three-dimensional scaffold for iPSC-NPC differentiation.

4. Discussion

Here, we established a unique human glial cell line, GDC90, which exhibited a radial glial-like molecular signature, a polarized shape, and radially spreading processes. Compared with the other glial cell lines tested, GDC90 cells showed a higher affinity for iPSC-NPCs, consistent with a previous report indicating that various glioma cell lines have different affinities for NSCs [16]. Consistent with this higher affinity, GDC90 cells expressed more N-cadherin than the other glioma-derived cell lines. Considering that during mouse corticogenesis, N-cadherin is essential for the attachment between radial glial cells and migrating neurons [17], N-cadherin may contribute to the scaffolding function of GDC90 cells in our *in vitro* system. The molecular signature and scaffolding properties of the GDC90 cells suggest they share some characteristics with RG cells. Our findings support the possibility that RG cells are involved in human glioma development [18–20].

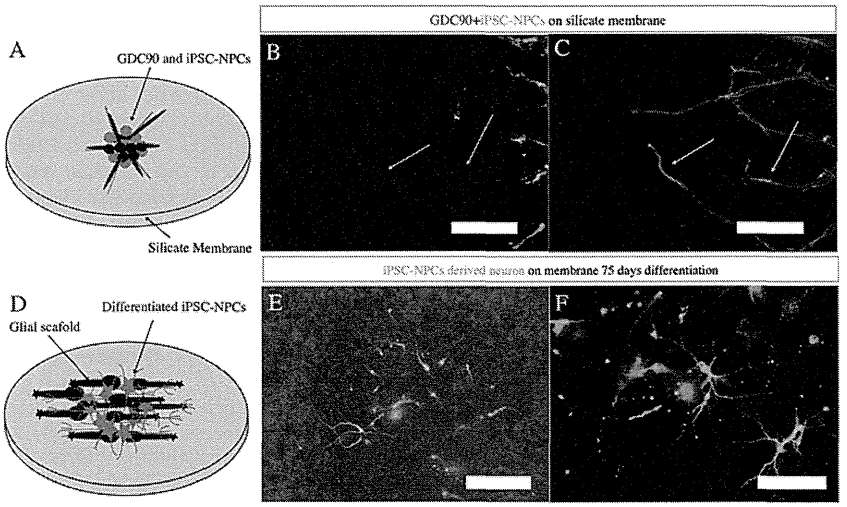

Fig. 4. Behavior of iPSC-NPCs co-cultured with GDC90 cells on a three-dimensional scaffold. (A–C) GDC90 cells directed iPSC-NPCs-derived neurite extension on a silicate fiber membrane. When GDC90 and iPSC-NPCs mixed aggregates were plated on the artificial membrane, iPSC-NPC neurites extended along the spreading GDC90 fibers. Scale bar: 100 μm. (D–F) Long-term co-culture of iPSC-NPCs and GDC90 cells on the silicate membrane. iPSC-NPCs became polarized and extended long neurites along the membrane fibers. Scale bar: 500 μm and 200 μm, respectively in E and F.

Co-culture of the fluorescently labeled cells showed that GDC90 cells could support the differentiation, polarization, and migration of iPSC-NPCs. Our findings suggest that the co-culture of RG-like GDC90 cells converts iPSC-NPCs to polarized neurons that migrate *in vitro*, consistent with a previous report showing that mouse neuronal migration *in vitro* required the presence of glial cells, which were prepared from fetal mouse brains or cultured neural stem cells [21,22]. Thus, our unique co-culture system enables *in vitro* modeling of the differentiation, polarization, and migration of iPSC-NPCs without *in vivo* xeno-transplantation procedures.

Non-vertebrate or lower vertebrate animals can reconstruct a functional CNS via RG cell activation prior to neurogenesis [23–25]. Here, we attempted to recapitulate this regenerative process on a three-dimensional scaffold. The co-culture of GDC90 cells and iPSC-NPCs on a silicate fiber membrane supported the extension of neurites from the iPSC-NPCs and the development of iPSC-NPC-derived polarized neurons that were capable of long-term survival. This membrane is so easy to handle that it may be technically possible to transplant this well-differentiated neuronal tissue. Conceptually, "glial-controlled regeneration" might provide a hint for regeneration of injured CNS. Although clinical applications will require the replacement of tumor-derived glial cells by iPSC-derived RGs [26,27], GDC90 or mitotically inactivated GDC90 cells will still be useful for basic research until advances in differentiation methods enable the reproducible, stable and abundant production of iPSC-derived RG cells.

5. Conclusion

We established a unique human glial cell line, GDC90, and examined its effects on iPSC-NPC differentiation, polarization, and migration. This simple technique has the potential to accelerate the research and development of iPSC-based disease modeling and regenerative medicine.

Acknowledgments

We thank all the members of Dr. Kanemura's and Prof. Okano's laboratories. This study was supported by the Research Center Network for Realization of Regenerative Medicine, Japan Science and Technology Agency (JST), the JSPS KAKENHI Grant Number 24592181, Japan, the Research on Applying Health Technology, Health and Labour Sciences Research Grants, the Ministry of Health, Labour and Welfare of Japan, and the Advanced Research for Medical Products Mining Programme of the National Institute of Biomedical Innovation (NIBIO).

Appendix A. Supplementary data

Supplementary data associated with this article can be found, in the online version, at http://dx.doi.org/10.1016/j.bbrc.2014.04.070.

References

[1] P. Rakic, Evolution of the neocortex: a perspective from developmental biology, Nat. Rev. Neurosci. 10 (2009) 724–735.
[2] X. Tang, L. Zhou, A.M. Wagner, M.C. Marchetto, A.R. Muotri, F.H. Gage, G. Chen, Astroglial cells regulate the developmental timeline of human neurons differentiated from induced pluripotent stem cells, Stem Cell Res. 11 (2013) 743–757.
[3] I. Espuny-Camacho, K.A. Michelsen, D. Gall, D. Linaro, A. Hasche, J. Bonnefont, C. Bali, D. Orduz, A. Bilheu, A. Herpoel, N. Lambert, N. Gaspard, S. Peron, S.N. Schiffmann, M. Giugliano, A. Gaillard, P. Vanderhaeghen, Pyramidal neurons derived from human pluripotent stem cells integrate efficiently into mouse brain circuits in vivo, Neuron 77 (2013) 440–456.
[4] M. Eiraku, K. Watanabe, M. Matsuo-Takasaki, M. Kawada, S. Yonemura, M. Matsumura, T. Wataya, A. Nishiyama, K. Muguruma, Y. Sasai, Self-organized formation of polarized cortical tissues from ESCs and its active manipulation by extrinsic signals, Cell Stem Cell 3 (2008) 519–532.
[5] Y. Shi, P. Kirwan, J. Smith, H.P. Robinson, F.J. Livesey, Human cerebral cortex development from pluripotent stem cells to functional excitatory synapses, Nat. Neurosci. 15 (477–486) (2012) S471.
[6] M.A. Lancaster, M. Renner, C.A. Martin, D. Wenzel, L.S. Bicknell, M.E. Hurles, T. Homfray, J.M. Penninger, A.P. Jackson, J.A. Knoblich, Cerebral organoids model human brain development and microcephaly, Nature 501 (2013) 373–379.
[7] A. Falk, P. Koch, J. Kesavan, Y. Takashima, J. Ladewig, M. Alexander, O. Wiskow, J. Tailor, M. Trotter, S. Pollard, A. Smith, O. Brustle, Capture of neuroepithelial-like stem cells from pluripotent stem cells provides a versatile system for in vitro production of human neurons, PLoS ONE 7 (2012) e29597.
[8] Y. Imaizumi, Y. Okada, W. Akamatsu, M. Koike, N. Kuzumaki, H. Hayakawa, T. Nihira, T. Kobayashi, M. Ohyama, S. Sato, M. Takanashi, M. Funayama, A. Hirayama, T. Soga, T. Hishiki, M. Suematsu, T. Yagi, D. Ito, A. Kosakai, K. Hayashi, M. Shouji, A. Nakanishi, N. Suzuki, Y. Mizuno, N. Mizushima, M. Amagai, Y. Uchiyama, H. Mochizuki, N. Hattori, H. Okano, Mitochondrial dysfunction associated with increased oxidative stress and alpha-synuclein accumulation in PARK2 iPSC-derived neurons and postmortem brain tissue, Mol. Brain 5 (2012) 35.
[9] K. Takahashi, K. Tanabe, M. Ohnuki, M. Narita, T. Ichisaka, K. Tomoda, S. Yamanaka, Induction of pluripotent stem cells from adult human fibroblasts by defined factors, Cell 131 (2007) 861–872.
[10] T. Shofuda, D. Kanematsu, H. Fukusumi, A. Yamamoto, Y. Bamba, S. Yoshitatsu, H. Suemizu, M. Nakamura, Y. Sugimoto, M.K. Furue, A. Kohara, W. Akamatsu, Y. Okada, H. Okano, M. Yamasaki, Y. Kanemura, Human decidua-derived mesenchymal cells are a promising source for the generation and cell banking of human induced pluripotent stem cells, Cell Med. 4 (2013) 125–147.
[11] Y. Kanemura, H. Mori, S. Kobayashi, O. Islam, E. Kodama, A. Yamamoto, Y. Nakanishi, N. Arita, M. Yamasaki, H. Okano, M. Hara, J. Miyake, Evaluation of in vitro proliferative activity of human fetal neural stem/progenitor cells using indirect measurements of viable cells based on cellular metabolic activity, J. Neurosci. Res. 69 (2002) 869–879.
[12] H. Niwa, K. Yamamura, J. Miyazaki, Efficient selection for high-expression transfectants with a novel eukaryotic vector, Gene 108 (1991) 193–199.
[13] S. Marchenko, L. Flanagan, Transfecting human neural stem cells with the Amaxa Nucleofector, J. Vis. Exp. 6 (2007) 240.
[14] Y. Nakamura, M. Yamamoto, E. Oda, A. Yamamoto, Y. Kanemura, M. Hara, A. Suzuki, M. Yamasaki, H. Okano, Expression of tubulin beta II in neural stem/progenitor cells and radial fibers during human fetal brain development, Lab. Invest. 83 (2003) 479–489.
[15] A. De Rosa, S. Pellegatta, M. Rossi, P. Tunici, L. Magnoni, M.C. Speranza, F. Malusa, V. Miragliotta, E. Mori, G. Finocchiaro, A. Bakker, A radial glia gene marker, fatty acid binding protein 7 (FABP7), is involved in proliferation and invasion of glioblastoma cells, PLoS ONE 7 (2012) e52113.
[16] O. Heese, A. Disko, D. Zirkel, M. Westphal, K. Lamszus, Neural stem cell migration toward gliomas in vitro, Neuro Oncol. 7 (2005) 476–484.
[17] M. Shikanai, K. Nakajima, T. Kawauchi, N-cadherin regulates radial glial fiber-dependent migration of cortical locomoting neurons, Commun. Integr. Biol. 4 (2011) 326–330.
[18] T.M. Kim, W. Huang, R. Park, P.J. Park, M.D. Johnson, A developmental taxonomy of glioblastoma defined and maintained by MicroRNAs, Cancer Res. 71 (2011) 3387–3399.
[19] Y. Liang, M. Diehn, N. Watson, A.W. Bollen, K.D. Aldape, M.K. Nicholas, K.R. Lamborn, M.S. Berger, D. Botstein, P.O. Brown, M.A. Israel, Gene expression profiling reveals molecularly and clinically distinct subtypes of glioblastoma multiforme, Proc. Natl. Acad. Sci. USA 102 (2005) 5814–5819.
[20] R. Mita, J.E. Coles, D.D. Glubrecht, R. Sung, X. Sun, R. Godbout, B-FABP-expressing radial glial cells: the malignant glioma cell of origin?, Neoplasia 9 (2007) 734–744
[21] U.E. Gasser, M.E. Hatten, Central nervous system neurons migrate on astroglial fibers from heterotypic brain regions in vitro, Proc. Natl. Acad. Sci. USA 87 (1990) 4543–4547.
[22] M.F. Santiago, S.S. Liour, R. Mendez-Otero, R.K. Yu, Glial-guided neuronal migration in P19 embryonal carcinoma stem cell aggregates, J. Neurosci. Res. 81 (2005) 9–20.
[23] M. Maden, L.A. Manwell, B.K. Ormerod, Proliferation zones in the axolotl brain and regeneration of the telencephalon, Neural Dev. 8 (2013) 1.
[24] V.S. Mashanov, O.R. Zueva, J.E. Garcia-Arraras, Radial glial cells play a key role in echinoderm neural regeneration, BMC Biol. 11 (2013) 49.
[25] M.M. Romero-Aleman, M. Monzon-Mayor, C. Yanes, D. Lang, Radial glial cells, proliferating periventricular cells, and microglia might contribute to successful structural repair in the cerebral cortex of the lizard *Gallotia galloti*, Exp. Neurol. 188 (2004) 74–85.
[26] R. Nat, M. Nilbratt, S. Narkilahti, B. Winblad, O. Hovatta, A. Nordberg, Neurogenic neuroepithelial and radial glial cells generated from six human embryonic stem cell lines in serum-free suspension and adherent cultures, Glia 55 (2007) 385–399.
[27] S.S. Liour, R.K. Yu, Differentiation of radial glia-like cells from embryonic stem cells, Glia 42 (2003) 109–117.

Published OnlineFirst October 1, 2014; DOI: 10.1158/0008-5472.CAN-14-0914

Molecular and Cellular Pathobiology

Cancer Research

IGF2 Preserves Osteosarcoma Cell Survival by Creating an Autophagic State of Dormancy That Protects Cells against Chemotherapeutic Stress

Takatsune Shimizu[1,2,3], Eiji Sugihara[2,3], Sayaka Yamaguchi-Iwai[2,4], Sakura Tamaki[5], Yuko Koyama[5], Walied Kamel[1,6,7], Arisa Ueki[2], Tomoki Ishikawa[2,8], Tatsuyuki Chiyoda[2], Satoru Osuka[2], Nobuyuki Onishi[2], Hiroko Ikeda[9], Junzo Kamei[9], Koichi Matsuo[6], Yumi Fukuchi[1], Toshihiro Nagai[10], Junya Toguchida[5,11,12], Yoshiaki Toyama[4], Akihiro Muto[1], and Hideyuki Saya[2,3]

Abstract

Osteosarcoma is a malignant bone tumor in children and adolescents characterized by intrinsic therapeutic resistance. The IGF2 is expressed at elevated levels in osteosarcoma after treatment with chemotherapy, prompting an examination of its functional contributions to resistance. We found that continuous exposure to IGF2 or insulin in the absence of serum created a dormant growth state in osteosarcoma cells that conferred resistance to various chemotherapeutic drugs *in vitro*. Mechanistic investigations revealed that this dormant state correlated with downregulation of downstream signaling by the IGF1 receptor, heightened cell survival, enhanced autophagy, and the presence of extracellular glutamine. Notably, inhibiting autophagy or depleting glutamine was sufficient to increase chemotherapeutic sensitivity in osteosarcoma xenografts in mice. Clinically, we confirmed that IGF expression levels were elevated in human osteosarcoma specimens from patients who received chemotherapy. Together, our results suggest that activation of IGF or insulin signaling preserves the survival of osteosarcoma cells under chemotherapeutic stress, providing a drug-resistant population that may engender minimal residual disease. Attenuating this survival mechanism may help overcome therapeutic resistance in osteosarcoma. *Cancer Res; 74(22); 6531–41. ©2014 AACR.*

[1]Department of Pathophysiology, School of Pharmacy and Pharmaceutical Sciences, Hoshi University, Shinagawa-ku, Tokyo, Japan. [2]Division of Gene Regulation, Institute for Advanced Medical Research, Keio University School of Medicine, Shinjuku-ku, Tokyo, Japan. [3]CREST, Japan Science and Technology Agency, Tokyo, Japan. [4]Department of Orthopedic Surgery, Keio University School of Medicine, Shinjuku-ku, Tokyo, Japan. [5]Department of Tissue Regeneration, Institute for Frontier Medical Sciences, Kyoto University, Sakyo-ku, Kyoto, Japan. [6]Laboratory of Cell and Tissue Biology, Keio University School of Medicine, Shinjuku-ku, Tokyo, Japan. [7]Faculty of Science, Mansoura University, Mansoura, Egypt. [8]Kasai R&D Center, Daiichi Sankyo Co. Ltd., Tokyo, Japan. [9]Department of Pathophysiology and Therapeutics, School of Pharmacy and Pharmaceutical Sciences, Hoshi University, Shinagawa-ku, Tokyo, Japan. [10]Electron Microscopy Laboratory, Keio University School of Medicine, Shinjuku-ku, Tokyo, Japan. [11]Department of Cell Growth and Differentiation, Center for iPS Cell Research and Application, Kyoto University, Sakyo-ku, Kyoto, Japan. [12]Department of Orthopaedic Surgery, Kyoto University Hospital, Sakyo-ku, Kyoto, Japan.

Note: Supplementary data for this article are available at Cancer Research Online (http://cancerres.aacrjournals.org/).

Corresponding Authors: Takatsune Shimizu, Department of Pathophysiology, School of Pharmacy and Pharmaceutical Sciences, Hoshi University, 2-4-41 Ebara, Shinagawa-ku, Tokyo 142-8501, Japan. Phone: 81-3-5498-5309; Fax: 81-3-5498-5916; E-mail: t-shimizu@hoshi.ac.jp; and Hideyuki Saya, Division of Gene Regulation, Institute for Advanced Medical Research, Keio University School of Medicine, 35 Shinanomachi, Shinjuku-ku, Tokyo 160-8582, Japan. Phone: 81-3-5363-3981; Fax: 81-3-5363-3982; E-mail: hsaya@a5.keio.jp

doi: 10.1158/0008-5472.CAN-14-0914

Introduction

Osteosarcoma is the most common nonhematogenous malignant bone tumor in children and adolescents. Death from osteosarcoma is largely attributable to the unchecked survival of a chemoresistant cells, and clinical outcomes have not changed substantially over the past 20 years (1–3). Characterization of the mechanisms of such chemoresistance will thus be a key to the development of novel therapeutic options.

The emergence of drug-resistant cancer cells has been attributed to stochastic events mostly associated with genetic mutations (4, 5). However, the mutation-based mechanism is thought to occur over a relatively long time period and may therefore not account for the rapid emergence of latent drug-tolerant cells. Instead, nonmutational alterations after the onset of therapy induced by the modified microenvironment also can give rise to a drug-tolerant state in cancer cells (4, 6, 7). Also importantly, resistant subpopulations of cancer cells, possibly identical to cancer stem cells, may initially be present within tumors, and their subsequent enrichment by therapy may be responsible for the recurrence of disease (8–10). Because pre-existing resistant subpopulations, such as cancer stem cells, have not yet been fully ascertained in osteosarcoma, elucidation of the molecular mechanisms underlying such

Published OnlineFirst October 1, 2014; DOI: 10.1158/0008-5472.CAN-14-0914

therapy-induced alterations in cancer will be important for the development of new treatments.

We recently developed a mouse model of osteosarcoma based on the overexpression of c-MYC in bone marrow stromal cells derived from *Ink4a/Arf* knockout mice. Injection of highly tumorigenic cells (designated AXT cells) into syngeneic mice results in the development of lethal osteosarcoma with metastatic lesions that mimics human osteoblastic osteosarcoma (11). We previously showed that cellular heterogeneity as well as therapeutic resistance in this model can be brought about by soluble factors released from the tumor microenvironment (12).

In the present study, we identified IGF2 as a soluble factor whose gene was expressed at an increased level in osteosarcoma tumors after chemotherapy. Despite its function as a growth factor, IGF2 ensured cell survival with arresting cell cycle and conferred a drug-tolerant state in osteosarcoma cells. These effects of IGF2 were mimicked by insulin. Our findings implicate IGF2 and possibly insulin signaling in the therapeutic resistance of osteosarcoma.

Materials and Methods

Human osteosarcoma samples

Osteosarcoma tissues were obtained from each patient at the time of biopsy (T1) and surgical resection after neoadjvant chemotherapy (T2). All patients received basically same chemotherapy, and all samples were approved for analysis by the ethics committee of the Faculty of Medicine, Kyoto University (Kyoto, Japan). Characteristics of each patient in detail are described in Table 1.

Cell culture

AXT cells and human SAOS2 and U2OS (ATCC) were maintained in IMDM (Life Technologies) supplemented with 10% FBS. For continuous exposure to mouse or human IGF2 (R&D Systems) or human insulin (Sigma-Aldrich), cells were incubated overnight in serum-containing medium, washed with serum-free medium, and cultured in DMEM containing high glucose supplemented with 2 mmol/L GlutaMAX (Life Technologies) and either 50 ng/mL IGF2 or 50 nmol/L insulin. Medium was replaced 3 times a week, and the cells were subjected to analyses at 12 hours after a medium change unless indicated otherwise.

Cell proliferation assay

Cell viability was measured with Cell Titer-Glo Assay kit (Promega). The detailed experimental scheme is shown in Supplementary Materials and Methods and Supplementary Fig. S1D.

Tumor xenograft model

All animal care and procedures were performed in accordance with the guidelines of Hoshi University (Tokyo, Japan) and Keio University. For establishment of tumor xenografts, AXT cells (1×10^6) were suspended in PBS and injected subcutaneously into 8-week-old female C57BL/6 mice (SLC) on day 0. The schedule of administration of drugs is described in Supplementary Materials and Methods.

Reverse transcription-PCR

For patient samples, total RNA was isolated using RNeasy Mini Kit (QIAGEN) and treated with a DNase-one kit (QIAGEN) to remove gDNA. Reverse transcriptase (RT) reaction was performed using 1 to 2 μg of total RNA with the SuperScript III First-Strand Synthesis System (Life Technologies) according to the manufacturer's instructions. Real-time PCR was performed in triplicate using SYBR Green reagent (Applied Biosystems). cDNA from human liver was obtained from Human MTC PanelI (Clontech). HOS cells were obtained from ATCC. The abundance of target mRNAs was determined relative to that of *ACTB* mRNA. For mouse samples, total RNA extraction, reverse transcription, and real-time PCR analysis was performed as described previously (12). Sets of primers for real-time PCR are listed in Supplementary Table S1.

RNAi

AXT cells were subjected to reverse transfection for 24 hours under serum-containing IMDM with Silencer Select siRNAs for *Atg7* (s92536 or s92538; siRNAs 1 and 2, respectively) or with a control siRNA (Life Technologies), each at a concentration of 50 nmol/L. The detailed experimental scheme is shown in Supplementary Materials and Methods and Supplementary Fig. S1E.

Flow cytometry

Cells were fixed for 1 day with ice-cold 70% ethanol, washed with PBS, and incubated for 1 hour on ice with Alexa Fluor 647–conjugated Ki67 antibody (Cell Signaling Technology). Then, cells were washed and suspended in PBS containing propidium iodide at 10 μg/mL and RNase A (Sigma-Aldrich). DNA damage was evaluated using Alexa Fluor 647–conjugated γH2AX antibody and an isotype control antibody according to the manufacturer's instructions (Cell Signaling Technology). At least 10,000 live cells were analyzed by FACS Verse (BD Biosciences). Data were analyzed with FlowJo software (Tree Star).

Time lapse imaging

AXT cells were cultured either in serum- or IGF2-containing medium for 1 or 8 days before analysis, respectively. Cells incubated in the IGF2-containing medium were also exposed to serum beginning at 17.75 hours after the onset of analysis. Images were obtained as previously described (13).

Immunoblot analysis

Cells were lysed with Laemmli sample buffer (Bio-Rad). For preparation of a tumor homogenate, small fragments were suspended in the same buffer and disrupted using Biomasher (Nippi) and ultrasonic treatment. Immunoblot analysis was performed as previously described (11, 12). Actin or α-tubulin was examined as a loading control.

Transmission electron microscopy

Sample preparation and acquisition of images was performed as described elsewhere (14).

Published OnlineFirst October 1, 2014; DOI: 10.1158/0008-5472.CAN-14-0914

Immunostaining

Immunohistochemical analysis was performed as previously described (11, 12) using antibodies to GFP (Santa Cruz Biotechnology) and LC3 (MBL). For immunofluorescent staining, cells were fixed with ice-cold acetone for 5 minutes for Ki67 and phospho-histone H2AX or 4% paraformaldehyde for 15 minutes for phospho-histone H3, respectively, washed 3 times with PBS, exposed to PBS containing 3% BSA for 1 hour, and stained with antibodies to Ki67, phospho-histone H2AX, or phospho-histone H3 (Cell Signaling Technology). Alexa Fluor 488, 555, or 594–conjugated secondary antibodies were purchased from Life Technologies. Nuclei were stained with TOTO3 (Life Technologies) or 4′,6-diamidino-2-phenylindole (DAPI; Vector Laboratories). Stained cells were observed with a confocal microscope (LSM510; Zeiss) or a fluorescence microscope.

Measurement of the activity of Gst

Gst activity was measured by Gst activity assay kit (Abcam). Values were divided by each cell number and the activity per cell was calculated.

Statistical analysis

All assays were performed at least in triplicate and data are presented as means ± SD and analyzed by the Student t test unless indicated otherwise.

Results

IGF2 ensures survival of osteosarcoma cells in the absence of serum

Environmental soluble factors are known to alter the characteristics of cells. To clarify the mechanisms underlying emergence of chemoresistance of osteosarcoma, the expression of various soluble factors was examined. After exclusion of highly expressed molecules without the treatment of chemotherapeutic agents, which were previously described (12), we found IGF2 as one of the candidates whose mRNA abundance was originally low but significantly upregulated after chemotherapy. The amount of *Igf1* mRNA was unaffected (Fig. 1A and Supplementary Fig. S1A). This effect was even more pronounced in tumor cells sorted by GFP, which was overexpressed in AXT cells but not observed in GFP-negative nontumor cells. Serum IGF2 level was significantly increased in tumor-bearing mice and further slight increase was induced by chemotherapy (Supplementary Fig. S1B). On the basis of these findings, we investigated the role of IGF2 in osteosarcoma cells.

We first examined the effect of IGF2 on cell proliferation. IGF2 slightly stimulated proliferation in the presence of serum (Fig. 1B). Whereas withdrawal of serum results in cell-cycle arrest followed by cell death, the addition of IGF2 was found to support AXT cell survival after serum withdrawal. Mitotic cells were scarcely observed in AXT cells cultured in the presence of IGF2 (Fig. 1C). Insulin and IGF1 share downstream signaling pathways with IGF2 (15), and they also supported the survival of AXT cells after serum withdrawal (Fig. 1D, data not shown). In contrast, FGF2 had no such effect. The human osteosarcoma cell lines SAOS2 and U2OS survived in the absence of serum to a greater extent than did AXT cells. Although mitotic cells or many surviving cells were detected even under serum-free condition for 3 or 10 days, respectively, in U2OS cells (Supplementary Fig. S1C); therefore, the effect of IGF2 was undervalued, the survival of both human cells was also significantly enhanced by the presence of IGF2 (Fig. 1E). These findings indicated that IGF2 and insulin ensure osteosarcoma cell survival under serum-free conditions.

Dormancy-like state induced by long-term exposure to IGF2 or insulin

All AXT cells were dead under serum-free condition within 10 days, whereas flow cytometric analysis of live cells revealed that the G_0–G_1 fraction and the proportion of Ki67-negative (nonproliferating) cells was significantly increased, whereas the S and G_2–M fractions were significantly decreased for AXT cells maintained in IGF2-containing medium compared with those maintained in serum-containing medium (Fig. 2A and B and Supplementary Fig. S2A–S2C). AXT cells that had been arrested in IGF2 medium reentered the cell cycle 24 hours after exposure to serum. Similar cell-cycle arrest and downregulation of Ki67 expression were apparent both in AXT cells exposed to insulin and in SAOS2 cells exposed to IGF2 (Fig. 2C and D and Supplementary Fig. S2D–S2F).

To clarify the effect of IGF2 on cell cycle at the single-cell level, we performed time-lapse video microscopy. AXT cells cultured in serum-containing medium proliferated rapidly to achieve confluence within 1 day with a doubling time of 462 ± 30.3 min ($n = 5$; Fig. 2E). In contrast, most cells cultured in the presence of IGF2 had not entered mitosis during observation for up to 19 hours, although some cells entered the cell cycle. The arrested cells progressed into mitosis after subsequent exposure to serum (Fig. 2E and Supplementary Movie S1). The abundance of cyclins was downregulated in the IGF2-treated cells; however, this downregulation was reversed on exposure of the cell to serum (Fig. 2F). The proteasome inhibitor bortezomib also partially restored cyclin levels in IGF2-treated cells (Supplementary Fig. S2G), suggesting the involvement of proteasome-mediated degradation. Similar to IGF2, insulin mediated the reversible downregulation of cyclin expression in AXT cells. Together, these findings suggested that continuous exposure to IGF2 or insulin in the absence of serum maintains survival under dormancy-like state of osteosarcoma cells.

Long-term exposure leads to attenuation of responsiveness to IGF2 in AXT cells

To gain insight into the mechanism underlying the dormancy-like state, we examined signaling downstream of the IGF1 receptor (IGF1R). Binding of ligands to IGF1R triggers activation of signaling by the PI3K–Akt pathway (15). Removal of serum resulted in the dephosphorylation of Akt as well as of p70S6K and S6 in 2 hours (Fig. 3A).

Published OnlineFirst October 1, 2014; DOI: 10.1158/0008-5472.CAN-14-0914

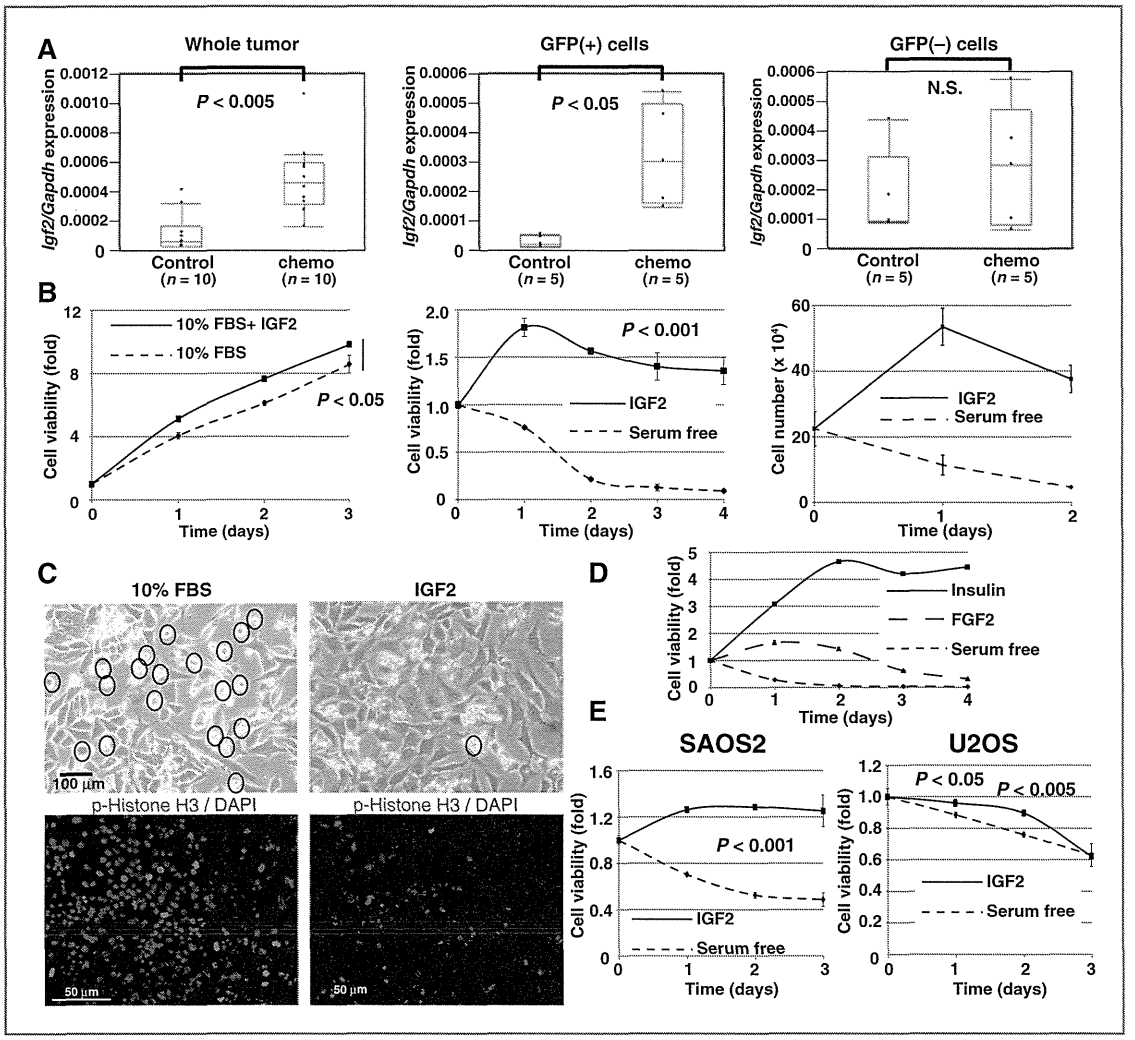

Figure 1. IGF2 ensures osteosarcoma cell survival under serum-free conditions. A, real-time PCR analysis of *Igf2* expression in AXT cell–derived subcutaneous tumors in mice subjected to chemotherapy. Data are presented as box-and-whisker plots for the indicated numbers of tumors. N.S., not significant. B, left and middle, cell viability of AXT cells cultured in medium containing serum either alone or together with mouse IGF2 or in serum-free medium with or without IGF2. Each ratio relative to the value for day 0 was calculated. Right, number of viable AXT cells cultured under serum-free condition with or without IGF2 for indicated days was counted. Live cells were evaluated by trypan blue exclusion. C, top, morphology of AXT cells maintained in the presence of serum or cultured in IGF2-containing medium for 6 days. Cells enclosed by circles are mitotic cells. Bottom, AXT cells cultured in the presence of serum or IGF2-containing medium for 5 days were stained with a phospho-histone H3 antibody and DAPI. D, viability of AXT cells cultured in serum-free medium with or without FGF2 (20 ng/mL) or insulin. E, viability of SAOS2 or U2OS cells cultured in serum-free medium with or without human IGF2.

Exposure of the serum-deprived cells to IGF2 induced a transient increase in the phosphorylation levels of these proteins, which had started to decline by 3 hours. To determine whether the transient nature of these effects of IGF2 was due to a loss of activity, we refreshed the IGF2-containing medium for the final 30 minutes of each incubation. However, such replenishment of IGF2 did not restore the phosphorylation levels of Akt and, more clearly, p70S6K and S6 at 12 hours (Fig. 3A). This attenuation of responsiveness was also apparent in cells cultured for 3 days under the presence of IGF2 (Fig. 3B). These cells fully responded to IGF2 24 hours after the final supplement of IGF2. However, this activation was rapidly downregulated and subsequent replenishment could not lead to the same level of activation of p70S6K and S6 as the initial response (Fig. 3B). Notably, downregulation of signaling apparent in cells cultured in the presence of IGF2 or insulin for 7 days was fully reversed by exposure of the cells to serum (Fig. 3C). We obtained